RESEARCH ARTICLE

Data-driven multi-scale mathematical modeling of SARS-CoV-2 infection reveals heterogeneity among COVID-19 patients

Shun Wang[1,2], **Mengqian Hao**[1,2], **Zishu Pan**[3], **Jinzhi Lei**[4]*, **Xiufen Zou**[1,2]*

1 School of Mathematics and Statistics, Wuhan University, Wuhan, China, **2** Hubei Key Laboratory of Computational Science, Wuhan University, Wuhan, China, **3** State Key Laboratory of Virology, College of Life Sciences, Wuhan University, Wuhan, China, **4** School of Mathematical Sciences, Center for Applied Mathematics, Tiangong University, Tianjin, China

* jzlei@tiangong.edu.cn (JL); xfzou@whu.edu.cn (XZ)

Abstract

Patients with coronavirus disease 2019 (COVID-19) often exhibit diverse disease progressions associated with various infectious ability, symptoms, and clinical treatments. To systematically and thoroughly understand the heterogeneous progression of COVID-19, we developed a multi-scale computational model to quantitatively understand the heterogeneous progression of COVID-19 patients infected with severe acute respiratory syndrome (SARS)-like coronavirus (SARS-CoV-2). The model consists of intracellular viral dynamics, multicellular infection process, and immune responses, and was formulated using a combination of differential equations and stochastic modeling. By integrating multi-source clinical data with model analysis, we quantified individual heterogeneity using two indexes, i.e., the ratio of infected cells and incubation period. Specifically, our simulations revealed that increasing the host antiviral state or virus induced type I interferon (IFN) production rate can prolong the incubation period and postpone the transition from asymptomatic to symptomatic outcomes. We further identified the threshold dynamics of T cell exhaustion in the transition between mild-moderate and severe symptoms, and that patients with severe symptoms exhibited a lack of naïve T cells at a late stage. In addition, we quantified the efficacy of treating COVID-19 patients and investigated the effects of various therapeutic strategies. Simulations results suggested that single antiviral therapy is sufficient for moderate patients, while combination therapies and prevention of T cell exhaustion are needed for severe patients. These results highlight the critical roles of IFN and T cell responses in regulating the stage transition during COVID-19 progression. Our study reveals a quantitative relationship underpinning the heterogeneity of transition stage during COVID-19 progression and can provide a potential guidance for personalized therapy in COVID-19 patients.

Author summary

Coronavirus disease 2019 (COVID-19) is currently destroying both lives and economies. However, patients infected with severe acute respiratory syndrome (SARS)-like

coronavirus (SARS-CoV-2) usually present heterogeneous and complicated progressions, such as different incubation periods (short and long), symptoms (asymptomatic and symptomatic) and severity (mild-moderate and severe). Currently, various clinical data and experimental data are available from different countries, which has great significance for integrating different types of data to comprehensively understand the diverse disease progression in COVID-19 patients and guide individual treatment strategies. Here, we developed a multi-scale computational model to describe the dynamical process of patients infected with SARS-CoV-2, including intracellular viral dynamics, multicellular infection process, and immune responses. By combining data integration, stochastic simulation and quantitative analysis based on the multi-scale mathematical model, we addressed an important question regarding how IFN response and T cell exhaustion quantitatively affect heterogeneous progression in patients with respect to incubation periods, symptoms and severity. Furthermore, the efficacy of various therapeutic strategies for treating COVID-19 patients with different severity degrees was evaluated and validated. The computational framework in this study can also be extended to explore the dynamical process of other coronavirus infections.

Introduction

Coronavirus disease 2019 (COVID-19), which is caused by the novel severe acute respiratory syndrome (SARS)-like coronavirus (SARS-CoV-2), is currently destroying global health and economies. Patients with COVID-19 exhibit different disease symptoms, including mild, moderate and severe cases [1, 2]. The severity of disease in infected individuals correlates with the numbers of immune cells (CD4$^+$ and CD8$^+$ T cells, B cells and natural killer cells [3], as well as serum levels of pro-inflammatory cytokines (IL-6, TNF, etc.) characterized as a cytokine storm [1, 2, 4, 5]. Importantly, the diverse incubation periods of SARS-CoV-2 infection in different patients make it incredibly difficult to predict the disease progression or to initiate clinical treatment on time [6, 7]. The mean incubation period of SARS-CoV-2 is estimated to be 3–7 days [8, 9], and asymptomatic COVID-19 patients effectively transmit SARS-CoV-2 during their incubation periods [10].

There are many cellular and molecular factors that influence COVID-19 severity. Angiotensin-converting enzyme-2 (ACE2), the functional receptor of SARS-CoV-2, plays a crucial role in the pathogenesis of COVID-19 by allowing viral entry into human cells [11]. ACE2 is highly expressed on target cells, including absorptive enterocytes and epithelial cells [11–13]. During viral infection, the spike (S) protein of CoV-2 interacts with ACE2, and the cellular transmembrane serine protease 2 (TMPRSS2) [14] mediates the viral envelope to host cell membrane fusion, leading to the release of viral nucleocapsid into the cytoplasm of host cells. After viral infection, cellular detection of viral replication is largely mediated by a family of intracellular pattern recognition receptors (PRRs) that sense aberrant RNA structures [15], resulting in the engagement of cellular antiviral defenses [16]. However, high IL-6 levels are associated with severe disease and death [17, 18], whereas the expression of interferon-γ (IFN-γ) tends to be slightly lower in severe cases than in moderate cases, primarily due to the decrease in CD4$^+$, CD8$^+$ T cells and NK cells [19]. Total T cells, and CD4$^+$ and CD8$^+$ T cell counts are negatively correlated with serum IL-6, IL-10, and TNF-α levels in COVID-19 patients, and patients in the disease resolution period exhibit decreased IL-6, IL-10, and TNF-α concentrations and restored T cell counts [20]. Therefore, IL-6 and IL-10 can be used as predictors for rapid prognosis of COVID-19 patients with higher risk of disease deterioration, and the neutrophil-to-

lymphocyte ratio and neutrophil-to-CD8+ T cell ratio have been identified as powerful predictors of severe COVID-19 [21].

COVID-19 progression involves multiple complex steps of virus-host interactions. COVID-19 in different individuals exhibits diverse severity, including asymptomatic and symptomatic, mild, severe and critical, etc. [22], suggesting that individual heterogeneity is important for understanding the mechanism of COVID-19 and designing personalized treatment. Usually, clinical and biological experiments are not well poised to explore individual heterogeneity. To better understand the relationship between individual heterogeneity and disease severity in COVID-19 patients and to identify more effective treatments for different patients, in this study, we developed a data-driven multi-scale mathematical model to predict the clinical course of SARS-CoV-2 infection and quantitatively explored the factors underlying COVID-19 disease severity. By combining differential equations with stochastic modeling, as validated through different sources of experimental, epidemiological, and clinical data, we analyzed individual heterogeneity using stochastic simulation and quantitative analysis. Our results will contribute to understanding COVID-19 disease heterogeneity and to identifying novel clinical therapies.

Results

Host immune responses associated with COVID-19 severity based on multiple data analysis

To investigate host immune responses in COVID-19, we collected multiple datasets with adaptive immune cell counts, cytokines levels, proteomics, and single cell RNA-sequencing from COVID-19 patients with different symptoms (see Methods). First, we examined T cell response by comparing the counts of T cell subsets between 50 healthy donors and 157 COVID-19 patients (117 moderate and 40 severe symptoms) from Yale New Haven Hospital (Dataset 4) (Fig 1a–1d). The percentage of naïve CD4+ and CD8+ T cells were not significantly different between healthy donors and in severe patients (Fig 1a and 1b). Both CD4+ and CD8+ T cells exhibited significantly lower levels in patients than in healthy donors, and severe patients presented even lower level than that in moderate patients (Fig 1c and 1d).

Previous studies have shown that the reduction in T lymphocytes is linked to T cell exhaustion [19]. We examined the expression of the marker gene Tim-3 for T cell exhaustion in 41 COVID-19 patients from the Fifth Medical Center of PLA General Hospital of China (Dataset 2). The percentage of CD4+ and CD8+ T cells expressing Tim-3 on their surface was significantly higher in severe patients than in mild patients (Fig 1e and 1f). We further analyzed the distribution of Tim-3 transcription based on single cell RNA-sequencing data from 8 moderate patients and 13 critical patients from Charité-Universitätsmedizin Berlin and University Hospital Leipzig (Dataset 5). Critical patients exhibited significantly increased frequencies of cytotoxic T lymphocytes (CTLs) and regulatory T cells (CD4+T/Treg), and elevated Tim-3 transcription levels (Fig 1g and 1h), implying increased higher level T cell exhaustion in critical patients [23]. These data analyses suggest that exhaustion of T cells is associated with the reduction of T cells and accelerates the malignant development of COVID-19.

Previous studies have shown that a cytokine storm in COVID-19 may result in the emergence of severe patients and increase mortality [24–26]. We analyzed the published data of cytokine levels in COVID-19 patients from Datasets 3 and 4. The cytokines IL-6, IL-10, and IFN-γ were present at markedly higher levels in nonsurvivors patients than in survivors from the data of Renmin Hospital of Wuhan University (Fig Aa-c in S1 Text), and exhibited obvious increases from healthy donors and moderate patients, to severe patients from data of the Yale New Haven Hospital (Fig Ad-f in S1 Text). These results suggest that higher level cytokines
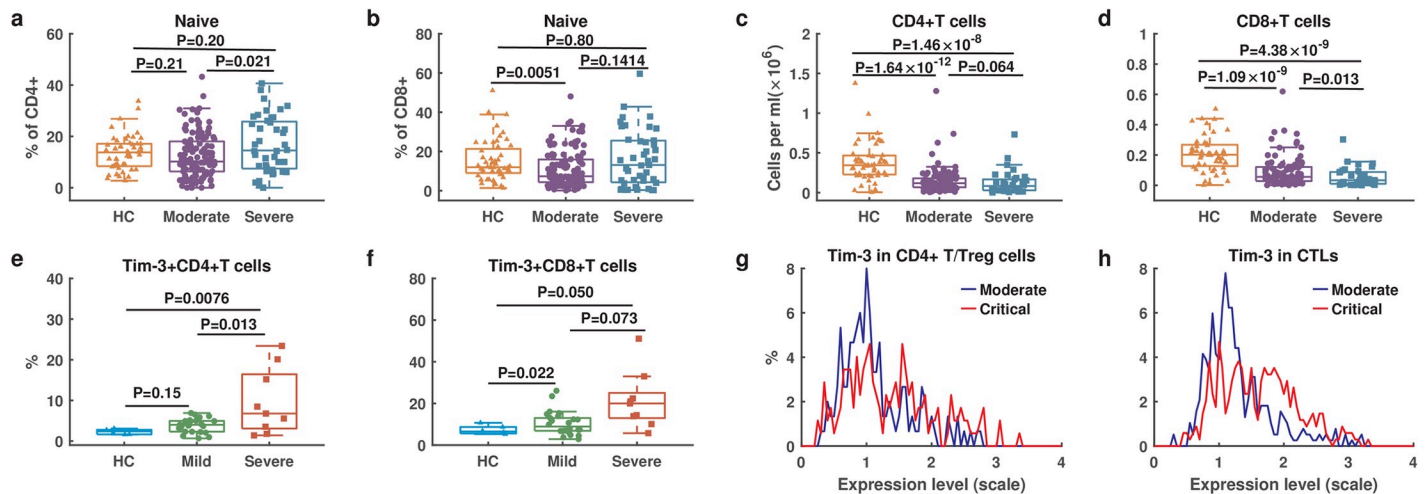
Fig 1. Multiple data on T cell response from COVID-19 patients with different symptoms. a. The percentage of naïve CD4+ T cells over CD4+ T cells. **b**. The percentage of naïve CD8+ T cells over CD8+ T cells. **c**. Counts of CD4+ T cells. **d**. Counts of CD8+ T cells. **a-d** include healthy control (HC: n = 50), moderate (n = 117) and severe (n = 40) patients from Yale New Haven Hospital (Dataset 4). **e**. The percentage of Tim-3 expression on CD4+ T cells. **f**. The percentage of Tim-3 on CD8+ T cells. **e-f** include healthy control (HC: n = 6), mild (n = 29) and severe (n = 12) patients from the Fifth Medical Center of PLA General Hospital of China (Dataset 2). **g**. The distribution of Tim-3 expression levels in CD4+ T/Treg cells. **h**. The distribution of Tim-3 expression levels in cytotoxic T lymphocytes (CTLs). **g-h** include moderate (n = 8) and critical (n = 13) patients from Charité-Universitätsmedizin Berlin and University Hospital Leipzig (Dataset 5). Significance was determined by two-sided, Wilcoxon rank-sum test.

https://doi.org/10.1371/journal.pcbi.1009587.g001

such as IL-6, IL-10, and IFN-γ are associated with severe symptoms and death cases in COVID-19 patients [27]. Additional integrative data analysis is shown in Figs B and C in S1 Text (Section 1 in S1 Text for the detailed description).

Based on the above data analysis, we proposed three assumptions in model development: (1) the depletion of T cell counts is associated with T cell exhaustion; (2) T cell exhaustion is dependent on the density of cytokines because persistently high cytokine levels is known to induce T cell exhaustion [28]; (3) the comprehensive effect of IL-6, IL-10, and IFN-γ is represented by a single variable of cytokines, but the complex network that regulates cytokines activities is currently not well understood and is not included in this study.

A multi-scale model of SARS-CoV-2 infection dynamics and host immune responses

To investigate disease progression in patients infected with SARS-CoV-2, we established a computational model that includes various scale dynamics. The model includes viral infection, viral spreading among multiple cells, and immune responses through IFN response, cytokines and effector T cells (Fig 2). The intracellular viral dynamics describes molecular-level events within individual cells, including the infection, binding, entry, replication of SARS-CoV-2, and IFN response signaling pathways (Fig 2 Intracellular), whereas the multicellular infection process describes the infectious cell-to-cell transmissions and the immune response that involves interactions between infected cells, cytokines, and T cell activities (Fig 2 Intercellular). The progression and severity of COVID-19 are dominated by the population size of infected cells (Fig 2 Organism).

SARS-CoV-2 primarily infects susceptible cells through receptor proteins (ACE2, NRP1). The CoV spike glycoprotein (S protein) of SARS-CoV-2 binds to receptors on the cell surface with high affinity, and the genomic RNA is released into the target cell. Inside the target cell, SARS-CoV-2 RNA employs organelles and synthases to complete viral replication and
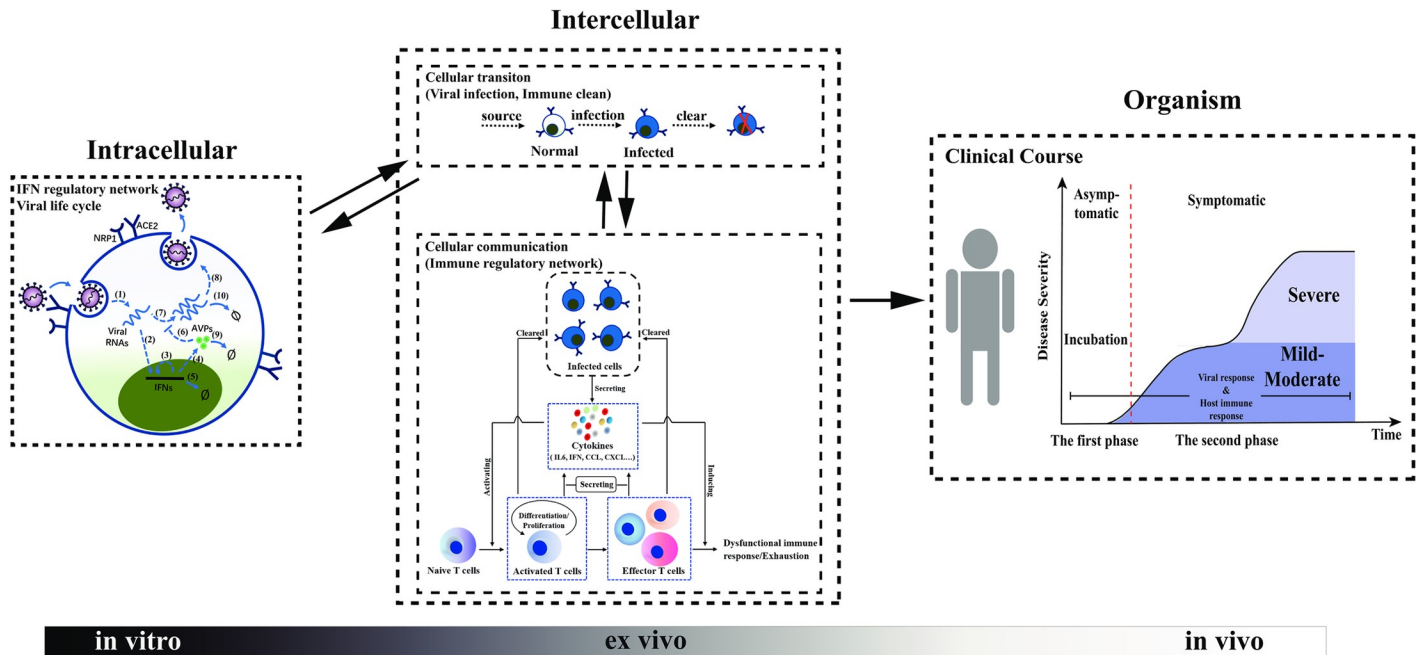
Fig 2. Framework of multiscale model of SARS-CoV-2 infection. Intracellular: The S protein of SARS-CoV-2 binds to receptor proteins (ACE2, NRP1) on the cell surface. Viral dynamics within a target cell are considered, which include (1) the release of RNA of SARS-CoV-2, (2) virus-activated IFN expression, (3) positive feedback of IFNs, (4) activation of AVPs by IFNs, (5) natural depletion of IFNs, (6) inhibition of the virus by AVPs, (7) viral RNA replication, (8) protein synthesis, assembly of novel SARS-CoV-2 and budding into the extracellular environment, (9) natural degradation of AVPs, and (10) degradation of viral RNA. The progeny viruses leave the target cell by budding and further infect additional susceptible cells. **Intercellular**: The status of target cells is divided into uninfected and infected. There is a supplied source of normal cells that will be transformed into infected cells if they are infected by the virus. The infected cell is identified and cleaned by effector T cells. With respect to cellular communication, T cells mediate the immune response to SARS-CoV-2. PRRs on the cell surface sense SARS-CoV-2 and activate the immune response. Immune cells secrete cytokines, such as IL-6, IL-10, IFN-γ, etc., and activate naïve T cells. The activated T cells undergo differentiation and proliferation, and emerge as effector T cells. Activated T cells and effector T cells clear the infected cells and secrete cytokines. Some of cytokines (pro-inflammatory cytokines) induce chronic inflammation, dysfunction of the immune response, and exhaustion of the effector T cells, which contribute to disease progression. **Organism**: The population size of infected cells dictates the progression and severity of COVID-19. The progression of COVID-19 is divided to two phases, symptomatic and asymptomatic. Furthermore, the severity of symptomatic patients is primarily divided into mild-moderate and severe.

assembly, which results in a large number of newly synthesized viruses. Upon viral replication, the interferon signaling pathway, one of the virus-mediated innate immune signaling pathways, is activated and engages type I interferons (IFNs) and antiviral proteins (AVPs), and to restrict the process of viral replication [29]. The newly synthesized virus leaves the target cell by means of budding, and other susceptible cells are further infected, forming a cascade of cell infection [30] (Fig 2 Intracellular).

Intracellular SARS-CoV-2 RNAs are recognized by host pattern recognition receptors (PRRs), which triggers activation of the host immune response. The active immune cells secrete cytokines, such as IL-6, IFN, etc., and activate the naïve T cells. The active T cells undergo differentiation and proliferation to produce a large amount of activated T cells and effector T cells. These cells continuously clear the infected cells, and secrete inflammatory cytokines, which may lead to chronic inflammation [31]. The inflammatory microenvironment further induces dysfunctional immune responses and exhaustion of effector T cells [28] (Fig 2 Intercellular).

Herein, a mathematical model was established to describe the time evolution of the number of infected cells and the host immune response in accordance with the above process. In the model, we considered a system of multiple cells (here we assumed a constant cell number N for simplicity) that are potential target cells of SARS-CoV-2. The cells are heterogeneous with

distinct levels of receptor proteins on their surface. Therefore, we have a set of $(4N + 1)$ differential equations, which describe the dynamics of intracellular virus RNA concentrations $X_{in}^i (i = 1, 2, \cdots, N)$, bounded cell surface receptor proteins $R^i (i = 1, 2, \cdots, N)$, IFN concentrations $[IFNs]^i (i = 1, 2, \cdots, N)$, AVP concentrations $[AVPs]^i (i = 1, 2, \cdots, N)$, and extracellular virus concentration X_{ex}. Moreover, the infected cells (cell number $N_{infected}$) promote the host immune response through the secretion of cytokines, which induces the production of effector T cells. The effector T cells clear the infected cells and secrete cytokines that induce further T cell exhaustion. The interactions among cytokine concentrations, effector T cells, and the infected cells are formulated as dynamic processes using two differential equations for among cytokine concentrations $[Cytokines]$ and the effector T cells number $[T_{effector}]$. Here, we assumed that the naïve T cells number remains constant throughout the process and that the total cell number is maintained at a constant level so that one uninfected cell is added to the system when an infected cell is cleaned by the effector T cells. The above assumptions lead to a system of $(4N + 3)$ differential equations for the multiple scale process from viral dynamics to immune responses (see the Methods section for the detailed mathematical model and formulations).

Based on the dynamic model, we introduced a ratio of infected cells (R_{IC}) to quantify disease progression after SARS-CoV-2 infection, which was defined as the ratio between the number of infected cells ($N_{infected}$) to total cells (N) in the model, i.e.,

$$R_{IC} = \frac{N_{infected}}{N}$$

A summary of key parameters and their biological significance, effects, and clinical/experimental evidences are listed in Table 1.

Progression dynamics of SARS-CoV-2 infection

To investigate the early stage dynamics of COVID-19 progression, we ran the model for 30 days after SARS-CoV-2 infection without considering of T cell exhaustion ($\rho = 0$) (Fig 3).

From numerical simulation, the ratio of infected cells (R_{IC}) remained low for a few days after SARS-CoV-2 infection, and most cases switched to a higher ratio of about 0.1~0.2 in 14 days. Nevertheless, there were also some cases that exhibited persistently low levels R_{IC} ($R_{IC} <$ 0.05) even 30 days after infection (Fig 3a). These results suggest the existence of two

Table 1. Summary of key parameters, biological significance, effects, and available clinical and/or experimental evidence.

Parameter	Description	Effect(s) on disease heterogeneity	Clinical and/or experimental evidence
K_1	IC50 of AVPs on the viruses	With K_1 increasing, R_{IC} develops potentially into asymptomatic state and T_{IP} could be prolonged	Asymptomatic infection is related to SARS-CoV-2 11083G>T mutation enhancing viral inhibitory effects on the antiviral state of the host [14, 45]
λ_2	The activation rate of IFNs induced by viruses	Enhancement of λ_2 prolongs T_{IP} and leads R_{IC} into asymptomatic state	Asymptomatic SARS-CoV-2 infected subjects display a very high serum type I IFN level [46]
ρ	The rate of T cell exhaustion	Increasing ρ leads to the switch of R_{IC} from mild-moderate into severe state; T_{IP} has no association with ρ	Elevated exhaustion level of T cells is present in severe patients [47]
K_4	EC50 of cytokines inducing T cell exhaustion	Decreasing K_4 promotes the switch of R_{IC} from mild-moderate into severe state	The cytokine storm may be responsible for increased PD-L1 expression (responding to decreased K_4 in our work), leading to CD8$^+$ T cell exhaustion [51]
$[T_0]$	Density of naïve T cells	Decreased $[T_0]$ results in R_{IC} developing into severe state and could shortens T_{IP}	Scarcity of naive T cells may be linked risk factors for severe COVID-19 [38]

Note: In our model, R_{IC} is the ratio of infected to total cells and T_{IP} is the simulated incubation period.
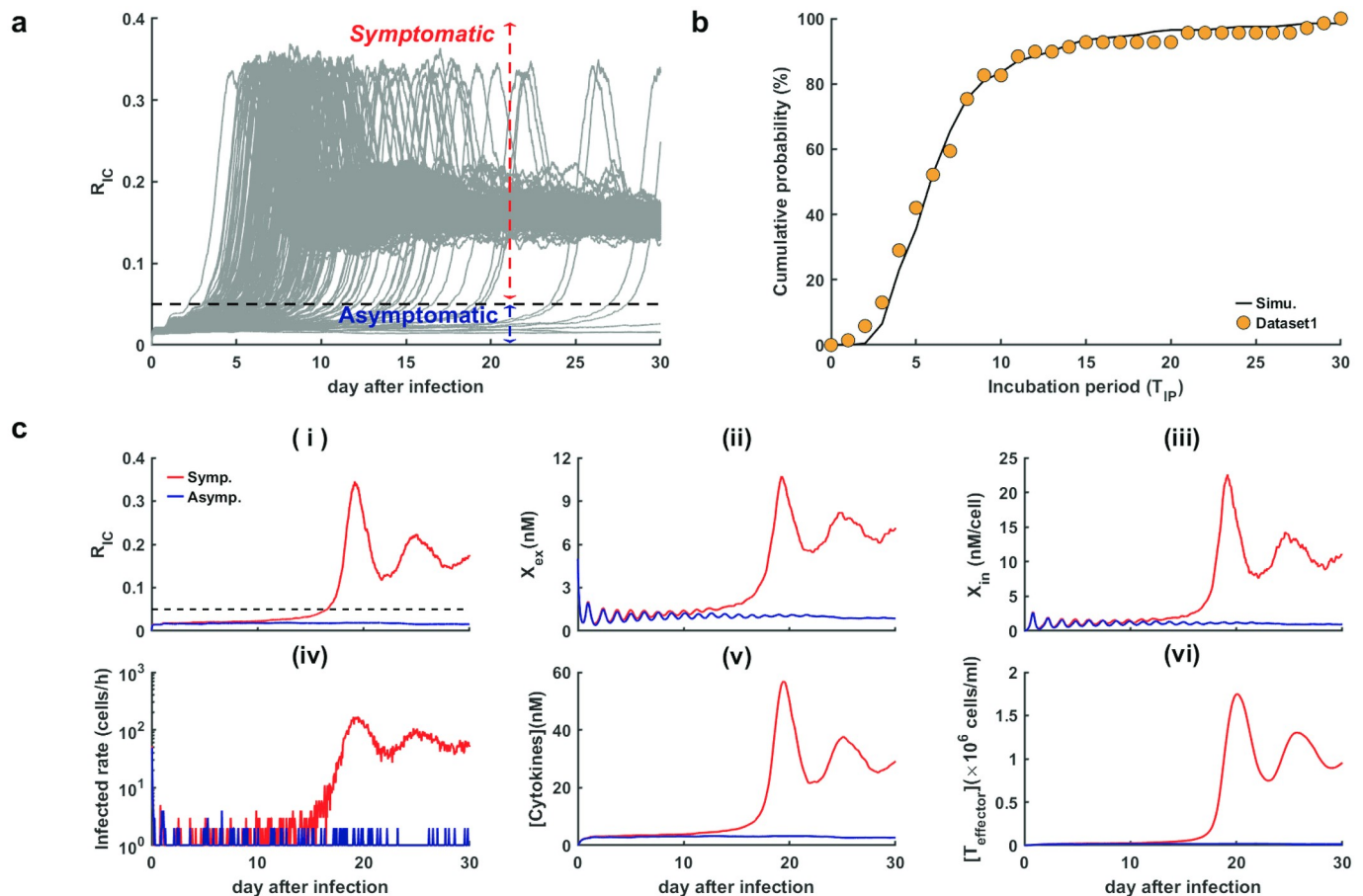
Fig 3. Progression dynamics in response to SARS-CoV-2 infection without considering T cell exhaustion ($\rho = 0$). a. Time course of the ratio of infected cells (R_{IC}) (out of 200 independent runs). The black dashed line is the threshold between the asymptomatic and symptomatic state. **b**. Comparison of incubation periods between simulations and real data in COVID-19. The black line shows the cumulative probability obtained from default values in Table A in S1 Text (out of 200 independent runs). The orange dots represent real data of incubation periods from Dataset 1. **c**. Two simulated trajectories were developed for the symptomatic and asymptomatic states (red and blue lines, respectively). (i)-(vi) respectively for the ratio of infected cells (R_{IC}), extracellular virus concentration (X_{ex}), intracellular virus concentration per cell (X_{in}), infected rate of susceptible cells, cytokine levels ([Cytokines]), and effector T cell counts ([$T_{effector}$]). Other parameters were assigned default values shown in Table A in S1 Text.

https://doi.org/10.1371/journal.pcbi.1009587.g003

subpopulations with markedly different dynamics of R_{IC}, who are either symptomatic ($R_{IC} \geq 0.05$) or asymptomatic ($R_{IC} < 0.05$). Hence, we introduced a threshold ($R_{IC} = 0.05$) to quantify the switch from symptomless to the state of presenting symptom after infection.

Clinically, COVID-19 patients exhibit incubation periods ranging from 2 to 14 days, with an average of 5–6 days, and rare patients present with longer periods of incubation greater than 14 days [31, 32]. Patients typically show no symptoms during the incubation period [30]. To verify the above threshold of R_{IC}, we defined the simulated incubation period (T_{IP}) of a patient as the time of R_{IC} increasing across the threshold value 0.05, i.e., $T_{IP} = \arg\max_{t}\{R_{IC}(t) \leq 0.05\}$. A simulation of 200 independent runs revealed good agreement between the cumulative probability of simulated incubation period and clinical data (Fig 3b). Hence, it is reasonable to distinguish between asymptomatic and symptomatic states using the threshold for the ratio of infected cells in the proposed model.

To further examine typical disease progression after SARS-CoV-2 infection, we selected two simulated trajectories developed for symptomatic and asymptomatic states, respectively,

over 30 days (Fig 3c). During the early stage, both symptomatic and asymptomatic cases displayed similar viral dynamics, with low levels of R_{IC} and virus concentrations inside and outside the cells (Fig 3c(i)–3c(iii)). Next, the extracellular virus concentration began to increase in the symptomatic sample (Fig 3c(ii)), along with the increasing of cell infection rate (Fig 3c(iv)), and the increasing of R_{IC} (Fig 3c(i)). The infected cell numbers and virus concentrations spiked when R_{IC} increased across the threshold and developed to a stationary symptomatic state in later stages. In contrast, the asymptomatic sample presented persistent low levels of infected cells and virus concentrations the entire time (Fig 3c(i)–3c(iii)). The immune responses showed a similar process of viral dynamics in that both cytokines levels and effector T cell numbers were maintained at low levels during the early stage and spiked to high levels in the symptomatic sample when R_{IC} increased across the threshold (Fig 3c(v) and 3c(vi)). These results reveal different dynamics in patients with symptomatic and asymptomatic clinical manifestations. We note that the non-zero steady states of R_{IC} and X_{ex} are inconsistent with clinical observations that some patients can recovery without treatment (Fig 3c(i) and 3c(ii)). This is because there are some other immune mechanisms that lead to the viral clearance are not included in the model. Therefore, in our simulations, we can consider the patients as viral clearance when the values of R_{IC} and X_{ex} are low enough.

Type I interferon modulates the transition from asymptomatic to symptomatic COVID-19

Type I interferon (IFN-I or IFN-α/β) is known to regulate patient response during the early stage after viral infection. Previous studies have shown that impaired interferon responses or inborn error type I IFN immunity may accelerate the clinical progression of patients infected with SARS-CoV-2 [33, 34]. To quantify the effects of type I IFN regulation, we varied the model parameters associated with viral replication (K_1) and the interferon activation (λ_2) to explore their effects on the switch from an asymptomatic to symptomatic state. The parameters K_1 and λ_2 associate with viral proteins, such as non-structure protein 6 (NSP6), which limits type I IFN synthesis and inhibits the establishment of an antiviral state based on the COVID-19 signaling pathways derived Kyoto Encyclopedia of Genes and Genomes (KEGG) [14]. In addition, sensitivity analysis showed that changes in K_1 and λ_2 were sensitive for the ratio of infected cells on day 30 after infection (Fig D and Section 3 in S1 Text for the detailed description).

To determine the influence of the IFN response preceding T cell exhaustion, we set $\rho = 0$, altered the parameters K_1 and λ_2, and performed 200 independent runs for each set of parameter values. First, we decreased K_1 or increased λ_2, respectively, according to the default values in Table A in S1 Text. For each simulated case, we examined the symptoms on day 30 and the incubation period (T_{IP}) (Fig 4a). When K_1 and λ_2 took default values ($K_1 = 47$, $\lambda_2 = 0.3$), more than 50% of simulated cases were symptomatic on day 5 after infection, and most cases developed into a symptomatic state on day 15 (Fig 4a, blue). When K_1 decreased ($K_1 = 45$), some simulated cases remained asymptomatic on day 30 after infection, and most of incubation periods for the symptomatic cases were prolonged in the range from 10 to 15 days, while a few were even longer than 25 days (Fig 4a, red). When λ_2 increased ($\lambda_2 = 0.35$), less than 20% of simulated cases were symptomatic at day 30, and the majority of incubation periods for the symptomatic cases were greater than over 15 days (Fig 4a, green). We further examined the simulated results with K_1 and λ_2 varied over a parameter range $40 \leq K_1 \leq 50$, $0.2 \leq \lambda_2 \leq 0.4$. The parameter range revealed three well separated domains according to symptoms on day 30, a symptomatic domain in which most patients developed into symptomatic (Fig 4b, red), an asymptomatic domain in which most patients remained asymptomatic on day 30 after
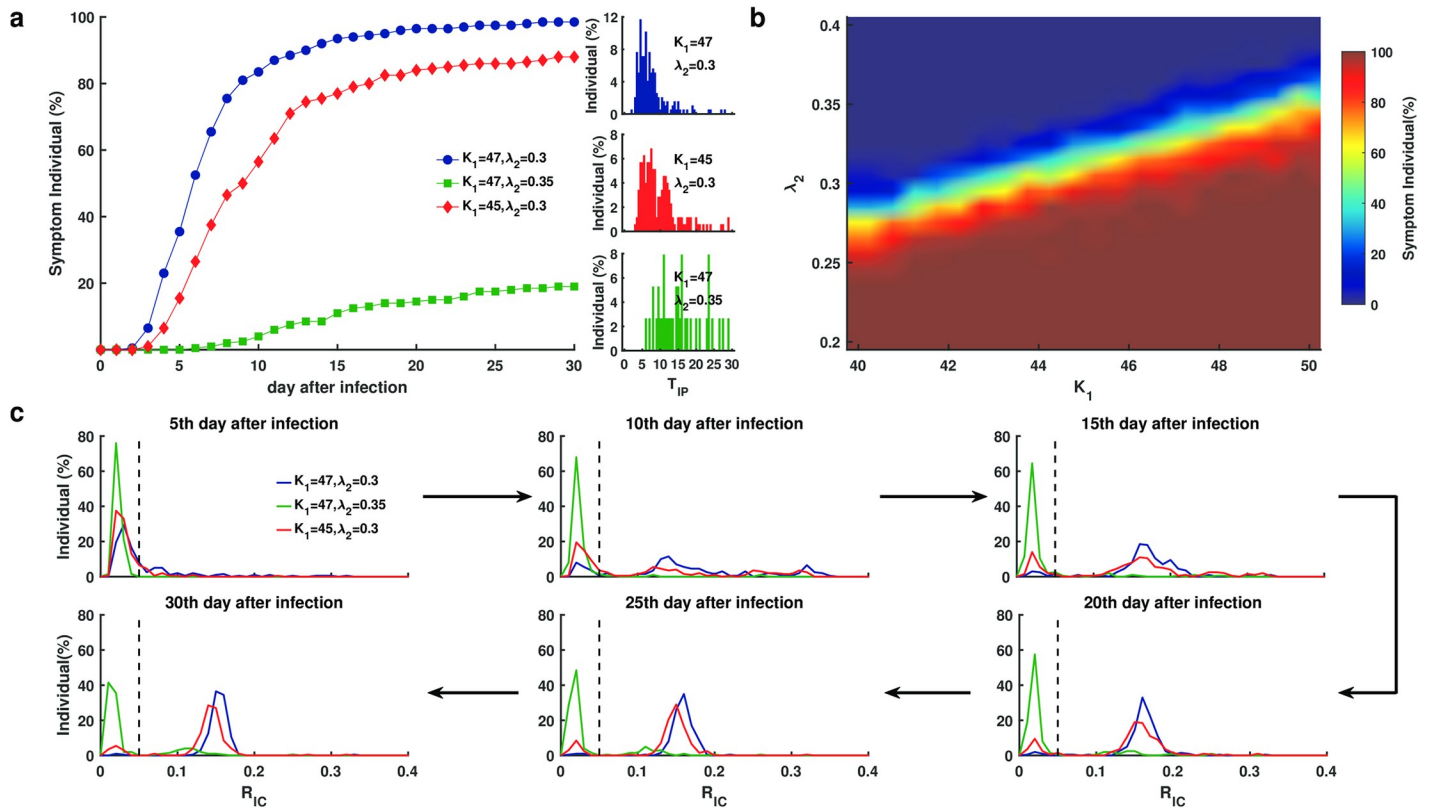
Fig 4. Disease evolution dynamics from asymptomatic and symptomatic states in response to SARS-CoV-2 infection without considering T cell exhaustion (ρ = 0). a. The percentage of cases (out of 200 independent runs) that developed into a state and the distribution of incubation period (T_{IP}) for various IC50 values of viral replication (K_1) and IFN response rate (λ_2) after infection. **b**. The distribution of symptomatic frequency. The color column indicates the percentage of symptomatic cases (out of 100 individual runs) when K_1 varies 40–50 and λ_2 varies 0.2–0.4. **c**. The distribution (fraction of individual) of R_{IC} at six different time points. The black dashed lines show the threshold separating asymptomatic and symptomatic states. Different color lines correspond to the IC50 of viral replication (K_1) and interferon response rate (λ_2). Other parameters were given default values as shown in Table A in S1 Text.

infection (Fig 4b, blue), and a bimodal region in which patients may show diverse transition dynamics from asymptomatic to symptomatic (Fig 4b). These results suggest that the IFN response is significant for the symptoms and incubation period of COVID-19 patients at early stages preceding T cell exhaustion.

To further explore the transition dynamics from asymptomatic to symptomatic states, we calculated the distribution of R_{IC} for all individuals on different days after infection. When the parameters were taken from the symptomatic region (K_1 = 47, λ_2 = 0.3) or the asymptomatic region (K_1 = 47, λ_2 = 0.35), most cases switched from $R_{IC} < 0.05$ to $R_{IC} \geq 0.05$ within 20 days (Fig 4c, blue) or remained $R_{IC} < 0.05$ on day 30 (Fig 4c, green). Nevertheless, when the parameters were taken from the bimodal region, the transition dynamics could be diverse, and the ratio R_{IC} exhibited an obvious bimodal distribution from days 10 to 30 after infection (Fig 4c, red). These results indicate different transition dynamics in patients with various IFN response. Except intracellular IFN-I response, we further explored the influence of intercellular T cell response on asymptomatic patient and incubation period. The result exhibited that increased number of naive T cells significantly prolonged the incubation period and raised the proportion of asymptomatic cases, while the incubation period and the proportion of asymptomatic cases were insensitive with T cell exhaustion (Fig E and Section 8 in S1 Text for the detailed description).
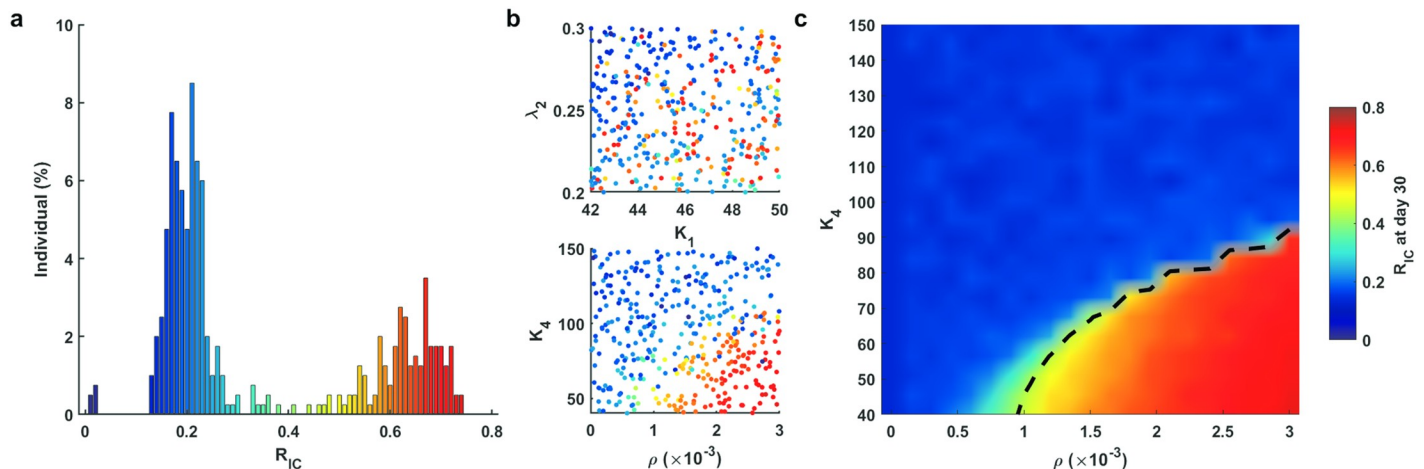
Fig 5. Bimorphism of patient symptoms. a. Distribution of R_{IC} on day 30 after SARS-CoV-2 infection. **b**. Scatterplot of varied parameters and R_{IC} on day 30. **c**. Distribution of the severity of COVID-19 patients. The color column shows R_{IC} at day 30 when K_4 varies between 40 and 150 and ρ varies within $[0, 3 \times 10^{-3}]$. The black dashed line shows the threshold between mild-moderate and severe cases. Other parameters assigned the default values shown in Table A in S1 Text.

https://doi.org/10.1371/journal.pcbi.1009587.g005

Characteristics of mild-moderate to severe symptoms in COVID-19 patients

COVID-19 patients exhibited distinct clinical manifestations in that 80% patients had only slight or mild symptoms, and some of them recovered by themselves, while 20% patients may further develop into severe situations where ventilators are required for survival [31, 35]. To explore the transition dynamics from mild-moderate to severe symptoms, we introduced the effect of T cells by setting $\rho > 0$, and varied the parameter K_4 that quantifies the exhaustion level of T cells.

We performed numerical simulation for 400 independent runs using the randomly selected parameters $42 \leq K_1 \leq 50$, $0.2 \leq \lambda_2 \leq 0.3$, $0 \leq \rho \leq 3 \times 10^{-3}$, and $40 \leq K_4 \leq 150$. The ratio of infected cells R_{IC} on day 30 for all runs exhibited an obvious bimodal distribution, corresponding to a high level ratio ($0.4 < R_{IC} < 0.8$) and a low level ratio ($0.05 < R_{IC} \leq 0.4$), respectively (we also noted a few cases with $R_{IC} \leq 0.05$, which corresponds to asymptomatic cases) (Fig 5a). These results suggest well defined mild-moderate and severe symptoms characterized by the ratio of infected cells, i.e., we refer to mild-moderate cases as those with $0.05 < R_{IC} \leq 0.4$, and severe cases as those with $0.4 < R_{IC} < 0.8$.

To investigate the key parameters that are significant for patient symptoms, we showed scatter plots for each case according to the parameter values and R_{IC} on day 30 (Fig 5b). Parameters values for both mild-moderate and severe cases were evenly distributed evenly in the (K_1, λ_2) plane, while they were well separated in the (ρ, K_4) plane, and severe cases primarily showed larger exhaustion rates ρ and smaller coefficients K_4. In the model, the parameters ρ and K_4 represented the effects of T cell exhaustion in later stage after SARS-CoV-2 infection. These results suggested that T cell exhaustion plays essential roles in the transition between mild-moderate and severe cases, which is consistent with clinical studies showing that impaired exhaustion features in SARS-CoV-2-reactive CD8^{+} T cells exist in on severe COVID-19 patients [36]. Some studies have shown that an impaired IFN response characterizes in severe or life-threatening patients [9, 33], and deficient IFN production can lead to the exhaustion of T cells, as T cell proliferation or T cell egress from lymphoid organs can be inhibited by delayed IFN response [37].
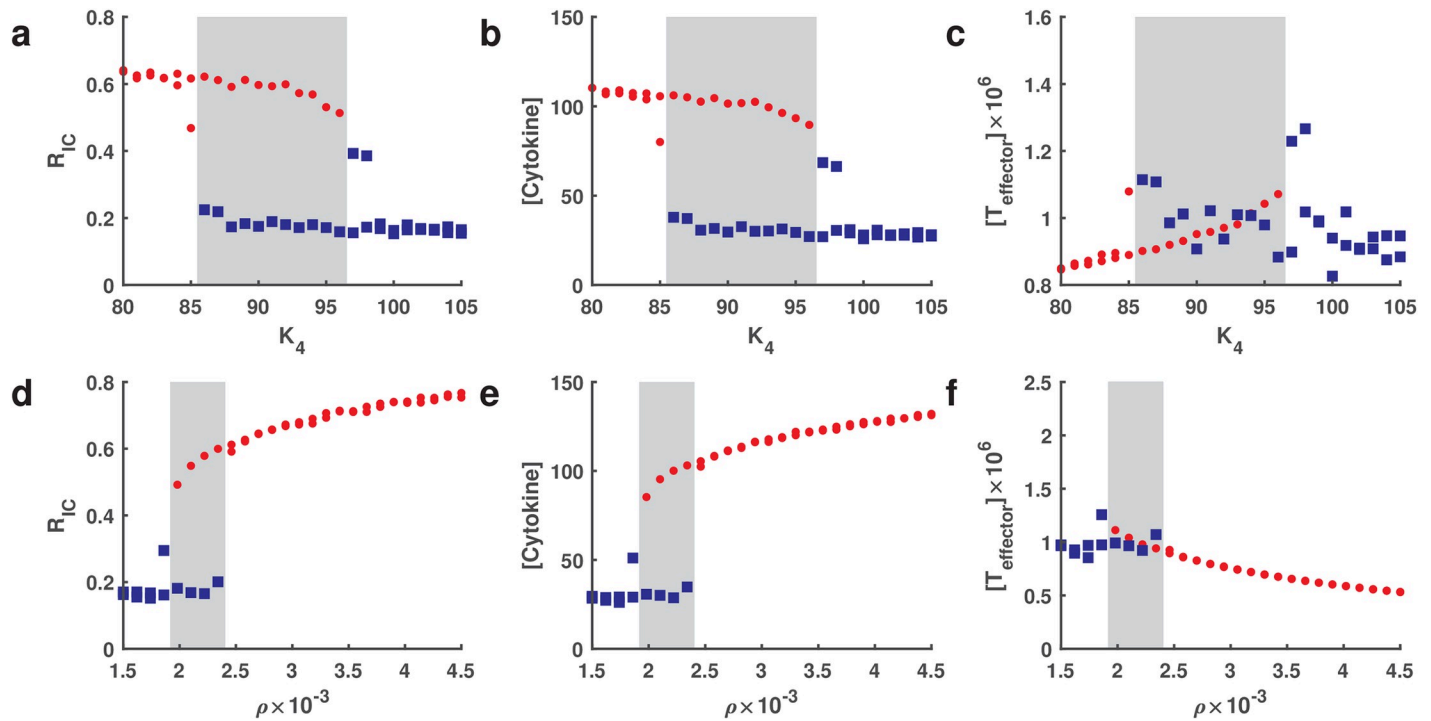
Fig 6. Bifurcation of parameter K_4 and ρ for R_{IC}, [Cytokines] and [T_{effector}] on day 30 after infection. a-c for parameter K_4 when the value of ρ is taken as 0.0025. **d-f** for parameter ρ when the value of K_4 is taken as 84. Red solid circles and blue squares represent severe and mild-moderate cases, respectively. The other parameters are default and are shown in Table A in S1 Text. The gray region indicates a bistable status for mild-moderate and severe cases.

To further identify the parameter values that characterize mild-moderate and severe cases, we took parameters ρ and K_4 over a range $0 \leq \rho \leq 3 \times 10^{-3}$, $40 \leq K_4 \leq 150$, and fixed other parameters to their default values shown in Table A in S1 Text. The dependence of R_{IC} on the parameters ρ and K_4 is shown in Fig 5c, illustrating good separation between mild-moderate and severe cases. We noted that the value of R_{IC} increased rapidly with increasing of ρ or decreasing of K_4. We further performed a bifurcation analysis of parameters ρ and K_4 related to T cell exhaustion (details in Section 6 in S1 Text). The result in Fig 6 demonstrated a bistable status for cytokines and R_{IC} in the range of $85 < K_4 < 98$ when ρ was taken as 0.0025 (Fig 6a and 6b). Similarly, a bistable region of ρ for cytokines and R_{IC} was in the range of $0.0018 < \rho < 0.0024$ when K_4 was taken as 84 (Fig 6d and 6e). These results imply that there is a risk of transition from mild-moderate to severe cases. Interestingly, the distribution of effector T cells was not similar to cytokines in the gray region (Fig 6c and 6f). In addition, we defined the first passage time from onset to severe cases and simulated the progression (details in Section 6 in S1 Text). The result indicated that the transition time decreases with increasing level of T cell exhaustion (ρ), while the transition time lengthens linearly when the level of anti-exhaustion of T cells (K_4) increases (Fig F in S1 Text). These results could be of great assistance for clinical prognosis in predicting subsequent clinical course in COVID-19 patients.

Activation and exhaustion of naïve T cells is related to the severity of COVID-19

Clinical studies have shown that age is associated with the development of severe COVID-19 [31], and further analysis of SARS-CoV-2-specific adaptive immune response during acute COVID-19 revealed that aging and scarcity of naïve T cells may be linked risk factors in severe
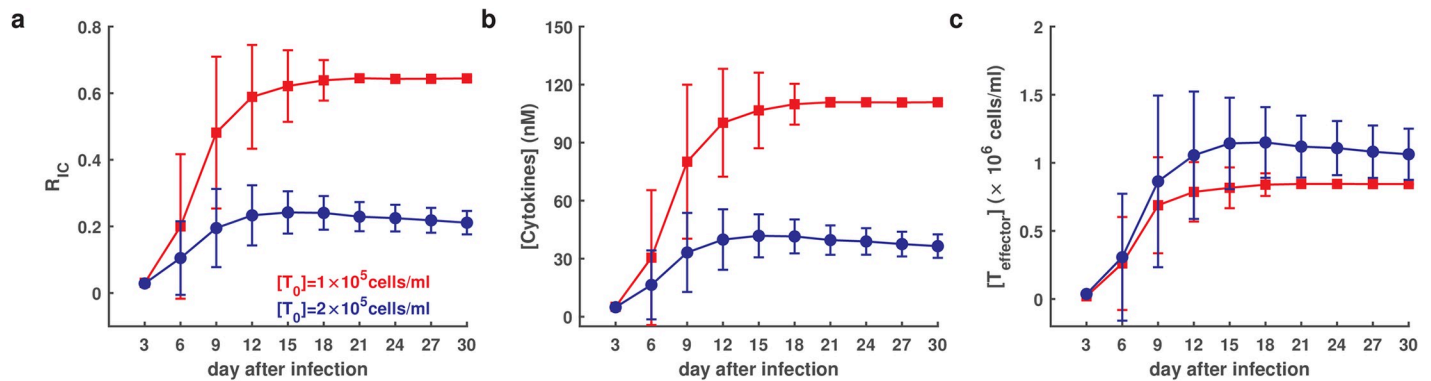
Fig 7. Dynamics of COVID-19 in response to a scarcity of naïve T cells and a mild exhaustion of T cells (ρ = 0.0005) (out of 100 individual runs). a. Time course of the average ratio of infected cells. **b.** Time course of average cytokines. **c.** Time course of average effector T cells. Red and blue lines indicate different levels of naïve T cells with ($[T_0] = 10^5$ cells/ml) and ($[T_0] = 2 \times 10^5$ cells/ml), respectively. The error bar indicates standard deviation. Other parameters were assigned default values as shown in Table A in S1 Text.

patients [38]. To quantify the effect of naïve T cell scarcity, we varied the naïve T cells number $[T_0]$ in the model to explore the dynamic of COVID-19 progression.

In simulations, we set $[T_0] = 2 \times 10^5$ cells/ml for a normal person, and $[T_0] = 1 \times 10^5$ cells/ml for a scarcity of naïve T cells, and the mild T cell exhaustion rate ρ = 0.0005, and performed 100 independent runs. The normal cases developed mild-moderate symptoms mild-moderate symptoms ($0.05 < R_{IC} < 0.4$), while naïve T cell scarcity cases developed into severe symptoms ($R_{IC} > 0.4$) (Fig 7a). Moreover, naïve T cell scarcity cases exhibited magnification of cytokine levels (Fig 7b) and reduced effector T cells (Fig 7c) compared to normal cases. These results indicate that a scarcity of naïve T cells may potentially lead to cytokine ectopic secretion and T cell reduction, which is supported by observations that decreased naïve T cell production with aging may result in an inappropriate inflammatory response, increasing the likelihood of a cytokine storm [39].

Treatment efficacy and prognosis of COVID-19 patients

The above numerical simulations reproduced the disease progression in patients infected with SARS-CoV-2. We further applied the model to evaluate the efficacy of different treatment methods, acceleration of IFN response (ε_1), restriction of viral replication (ε_2), promotion of extracellular virus clearance (ε_3), and inhibition of T cell exhaustion (ε_4) (details in Methods). We let a quadruple ($\varepsilon_1, \varepsilon_2, \varepsilon_3, \varepsilon_4$) represents a combination of the four types of treatments, and the quadruple (0, 0, 0, 0) indicates the control cases with no treatment. The efficacy of a treatment strategy was quantified by the relative reduction of the ratio of infected cells on day 30 after infection (clinical therapy starts on day 15), which is formulated as

$$E(\varepsilon_1, \varepsilon_2, \varepsilon_3, \varepsilon_4) = \frac{R_{IC}^{30}(0, 0, 0, 0) - R_{IC}^{30}(\varepsilon_1, \varepsilon_2, \varepsilon_3, \varepsilon_4)}{R_{IC}^{30}(0, 0, 0, 0)}$$

where $R_{IC}^{30}(\varepsilon_1, \varepsilon_2, \varepsilon_3, \varepsilon_4)$ represents the ratio of infected cells on day 30 after infection when treated with strategy ($\varepsilon_1, \varepsilon_2, \varepsilon_3, \varepsilon_4$). The efficacy takes a value from 0 to 1, and larger values indicate increased efficiency of the treatment strategy.

To compare the efficacy in patients with moderate or severe symptoms, we solved the model using different levels of T cell exhaustion in moderate (ρ = 0.0005) and severe (ρ = 0.0025) patients. For moderate patients, a single treatment of accelerating IFN response, restricting viral replication, or promoting viral clearance was highly efficient ($E > 0.8$), but
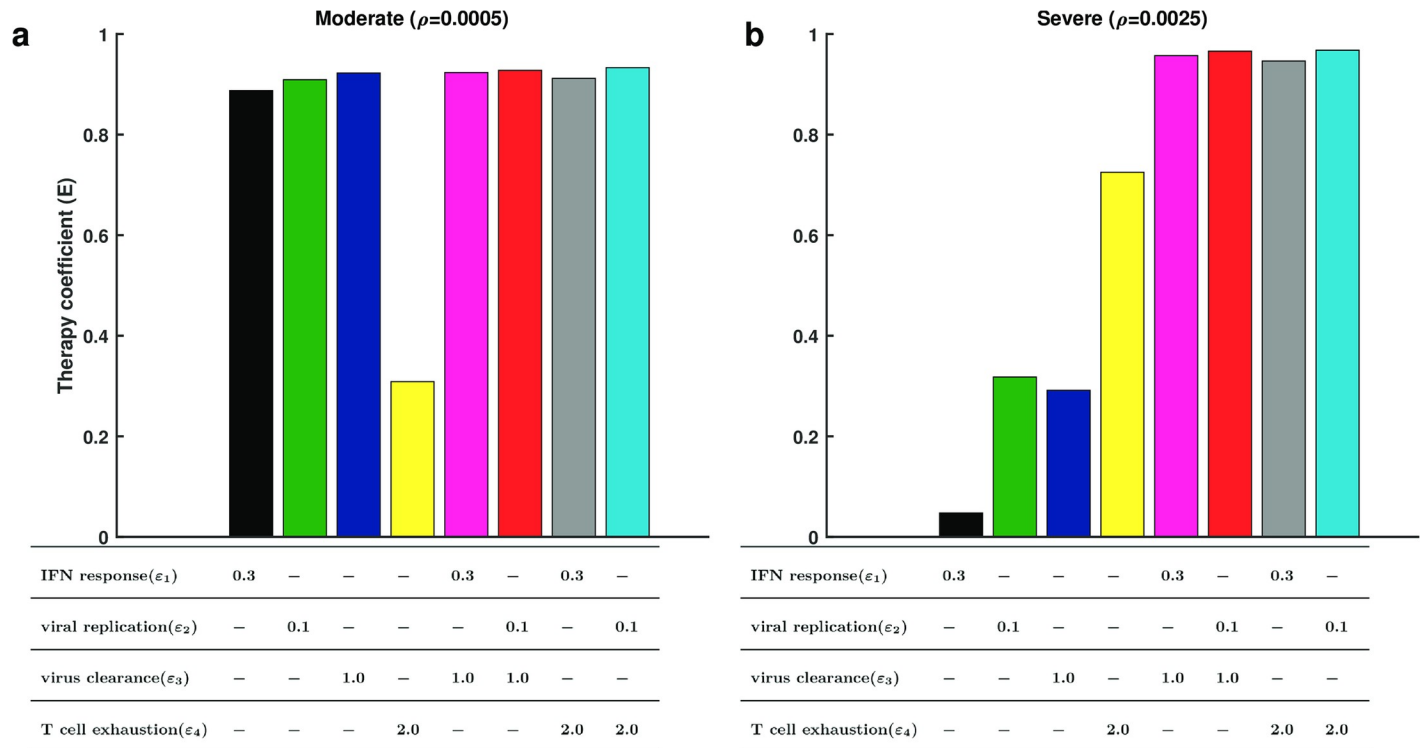
Fig 8. Comparison of the simulated efficacy for different treatment strategies in moderate and severe cases. a and **b** are the simulated efficacy of eight treatment strategies for moderate patients ($\rho = 0.0005$) and severe patients ($\rho = 0.0025$), respectively. Different colors correspond to treatment strategies. The table below the histogram shows the detailed values of the quadruple ($\varepsilon_1, \varepsilon_2, \varepsilon_3, \varepsilon_4$). "-" indicates that corresponding values are 0. Other parameters were given default values as shown in Table A in S1 Text.

https://doi.org/10.1371/journal.pcbi.1009587.g008

inhibition of T cell exhaustion alone exerted only marginal efficacy ($E \approx 0.3$) (Fig 8a), and the density of both cytokines and effector T cells were low (Fig G and Section 7.1 in S1 Text for the detailed description). For severe patients, however, inhibition of T cell exhaustion alone resulted in an efficacy of ($E > 0.6$) and a decreased concentration of cytokines (Fig Ga in S1 Text), while the other three methods alone yielded low efficacy ($E < 0.4$) (Fig 8b) and the density of neither cytokines nor effectors was changed (Fig Gb). In addition, we ran further simulations for drug efficacy using dose response curves (Fig H and Section 7.2 in S1 Text for the detailed description). The results indicated that the maximum efficacy of targeting IFN response (ε_1), viral replication (ε_2), and virus clearance (ε_3) was close to 1 (Fig Ha-c, He-g and Table B in S1 Text), but the maximum efficacy of targeting T cell exhaustion (ε_4) only reached 0.8 (Fig Hh and Table B in S1 Text) for severe case and was even less at 0.3 in moderate cases (Fig Hd and Table B in S1 Text), suggesting that antiviral treatment is more effective than immunological treatment for both moderate and severe cases. We fitted the dose response curves with Hill funcitons, and compared the Hill coefficient n and EC50 of the functions for moderate and severe cases in response to the same treatment strategy (Table B and Section 7.2 in S1 Text for the detailed description). The coefficient n in moderate cases was generally smaller than in severe cases, and the value of EC50 in severe cases was generally larger than in moderate cases, implying that moderate cases are more sensitive to treatment than severe cases, and higher doses are required for severe cases. These results suggest that antiviral treatment should be recommended for moderate patients, while for severe patients, inhibition of T
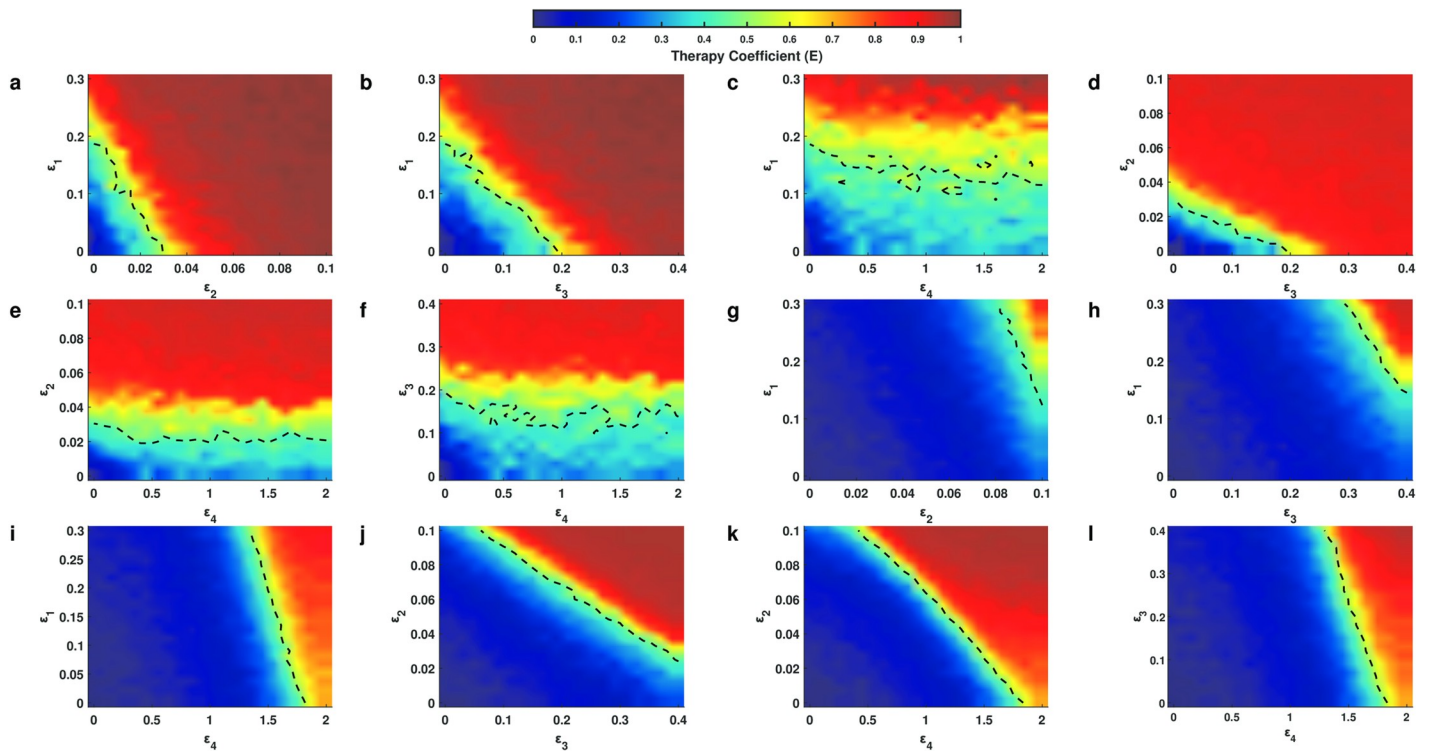
Fig 9. Therapeutic efficacy of united treatments for moderate and severe cases. a-f are combination of treatments for moderate cases. **g-l** are combination of treatments for severe cases. The dotted lines indicate half maximal efficacy. The colored bar is the therapeutic coefficient.

https://doi.org/10.1371/journal.pcbi.1009587.g009

cell exhaustion should be considered. Our results are in agreement with opinions that immune checkpoint inhibitors (ICIs) should be applied to treat severe COVID-19 patients [40, 41].

Moreover, for both moderate and severe patients, the combination of antiviral treatments (acceleration of IFN response, restriction of viral replication or promotion of virus clearance) and immune therapy (inhibition of T cell exhaustion) yielded highly efficiency for improving patient symptoms ($E > 0.8$) (Fig 8), and the density of both cytokines and effector T cells were low (Fig G in S1 Text). To quantify the relationship between therapeutic efficacy and combination therapy, we simulated different combinations in heterogeneous patients (Fig 9). On the one hand, the result of combination antiviral treatments (Fig 9a, 9b and 9d) demonstrated that the antiviral drugs could take less dose than EC50 (Table B in S1 Text) while maintaining high efficacy for moderate cases. The results from treatments for severe cases (Fig 9g, 9h and 9j) were similar to moderate cases, and the dose of antiviral treatment referred to the EC50 of a single antiviral treatment for moderate patients. These results suggest that a combination of treatments decreases drug dose while maintaining high efficacy for the treatment of COVID-19. On the other hand, the immunological treatment combined with any antiviral treatment did not result obvious improvements compared to the single antiviral treatment in moderate cases (Fig 9c, 9e and 9f), but combination of the EC50 of ε_4 in severe cases and low doses of other antiviral drugs maintained high levels of treatment efficacy in severe cases(Fig 9h, 9k and 9l), suggesting that the combination of immunological and antiviral treatments should be applied to treat severe cases.

Clinically, type I interferon treatment is a method of antiviral treatment for pathogenic human coronavirus infections [42], and medical use of Arbidol, an antiviral treatment, improves viral clearance and clinical outcomes in COVID-19 patients [43, 44]. To investigate

the dynamics of antiviral treatment, we simulated treatment dynamics by accelerating of IFN response ($\varepsilon_1 = 0.1$) and promoting of extracellular virus clearance ($\varepsilon_3 = 1.0$) for both moderate ($\rho = 0.0005$) and severe ($\rho = 0.0025$) cases. For single drug treatment, the ratio of infected cells for moderate cases rapidly decreased at the beginning of treatment and reached less than 0.05 (the threshold of the asymptomatic and symptomatic states) within 5 days after treatment (Fig Ia in S1 Text), however, for severe cases, the ratio of infected cells reduced more slowly and maintained the severe case ($0.4 < R_{IC} < 0.8$) on day 15 after treatment (Fig Ib in S1 Text). When combination of the two treatment strategies was applied, the ratio of infected cells in both moderate and severe cases reached less than 0.05 within 10 days after treatment (Fig I in S1 Text). These results illustrate the different dynamics of drug treatment for moderate and severe patients.

Discussion

Patients with COVID-19 exhibit marked individual heterogeneity in their disease progression. Quantitatively understanding how interactions between viral dynamics and host immune responses affect disease progression is important for clinical diagnosis and treatment. In this study, we developed a multi-scale mathematical model of the dynamics of SARS-CoV-2 infection. The model was established to describe the major biological processes associated with viral dynamics and host immune response, as well as the dynamics of infected cell populations in a viral microenvironment with respect to viral infection, viral replication, IFN response, viral budding, and immune clearance that appear in single cells (Fig 2 Intracellular). This model incorporates cross-talk among viral dynamics, cytokines and T cell responses with respect to the progression of COVID-19 (Fig 2 Intercellular). Multiscale simulations allowed us to quantify the heterogeneity of IFN responses (Fig 4) and T cell responses (Figs 5–7) that may result in the different severities of COVID-19. Heterogeneity plays an important role in the evolution of COVID-19 and lead to diverse disease progression in patients. The proposed model provides a method to quantify the therapeutic effects of potential treatment strategies in COVID-19 patients with different disease severities.

Numerical simulations demonstrate that IFN response is essential to modulate the transition from asymptomatic to symptomatic presentation and prolongs the incubation period (Fig 4a). We observed a diverse distribution of symptom presentation for heterogeneous IFN response from patients with COVID-19 (Fig 4b). Based on statistical analysis of genomic data from COVID-19 patients, asymptomatic infection is related to SARS-CoV-2 11083G>T mutation at residue 37 of non-structure protein 6 (NSP6) [45]. This mutation enhances viral stimulation of interferon and the expansion of viral inhibitory effects on the antiviral state of the host [14]. Quantitative study confirmed our simulation that patients with high levels of IFN response usually have asymptomatic manifestations [46]. These results can guide the disease management of patients in accordance with their responses in early stages after SARS-CoV-2 infections.

Many patients with COVID-19 appear to transition from mild-moderate to severe symptom in a short time, similar to a dynamic process of toggle switches between the two states. Clinical data have indicated significant differences in serum cytokines and active T cells in patients with mild-moderate and severe symptoms. Numerical simulations based on the proposed model revealed a bimorphism of symptoms that correspond to distinguished symptom manifestations of either a mild-moderate or severe state (Fig 5a). The transitions between mild-moderate and severe manifestation were closely associated with the model parameters quantifying the exhaustion of T cells (Figs 5 and 6 and Fig F in S1 Text). Clinically, elevated exhaustion level of T cells was present in severe patients [47], which is consistent with our

numerical results. In addition, we simulated the infection dynamics under a scarcity of naïve T cells, and found that a scarcity of naïve T cells leads to the severe state with high levels of cytokines and a reduction in effector T cells (Fig 7). The simulation results indicate a disruption in the balance between the exhaustion of T cells and cytokine production in restricting virus spreading. Under normal conditions, cytokines produced from both infected cells and T cells promote the generation of effector T cells from naïve cells. Moreover, increased of cytokines induces the exhaustion of T cells [48] to maintain a balance between cytokine secrete and T cell activation. Nevertheless, this balance can be broken due to a scarcity of naïve T cells, which leads to severe and even life-threatening cases.

Based on the disease progression obtained from our model, we suggest potential methods for treating patients with different symptoms. Single antiviral treatment is effective for patients with moderate symptoms, while immunotherapy and combination treatment should be considered for severe patients (Fig 8 and Figs G and H in S1 Text). The results of quantitative treatment for COVID-19 (Fig 9) suggest that a combined immunotherapy with antiviral drug could be a potential strategy for COVID-19 severe patients. The timing of drug administration is certainly important for the overall effects of combination therapy, and the problem of optimal drug administration protocol is beyond the current study. Clinically, most moderate patients are treated with antivirals, while many patients with severe symptom presentation are treated with combined treatment [49, 50], which in agreement with our treatment strategies for COVID-19 patients. We further modeled trajectories of two antiviral treatments, type I interferon and Arbidol [44], for moderate and severe patients (Fig I in S1 Text). Although it is difficult to make precise predictions in the absence of clinical trial data, our results highlight the efficacy of single antiviral treatment for moderate patients and the necessity of combination treatments for severe patients.

There have been many published and preprint reports of predictive mathematical models for the COVID-19 pandemic. These epidemiological models can be valuable for the prediction and controlling of disease spreading [52, 53]. Pharmacokinetic model is also applied to quantitatively predict treatment of drugs for COVID-19 [54]. Less attention has been paid to the predictive models of disease progression in heterogeneity outcome. Recently, a mechanistic, within-host ODE model was established to study the immune response to SARS-CoV-2 and the impact of delayed IFN on infection dynamics [55]. Virtual patient cohorts were generated based on an algorithm of random parameter sampling, and dynamics of how immune mechanisms drive disease outcomes was discussed. In our study, the stochastic and multiscale model was developed to consider the inherent heterogeneity of the infection process and the related clinical therapy dynamics. The multi-scale mathematical model proposed in this study was intended to establish a predictive model for disease progression from viral infection to patient symptoms and to provide quantitative understanding of the heterogeneous clinical courses in patients with COVID-19. For example, the process of IFN response and T cell response modulate the evolution of COVID-19 stage, from which potential clinical methods are suggested based on model simulations. The proposed model primarily incorporates viral dynamics with host immune response. Further interactions between cytokines and immune cells were omitted in the current model, which are important for the understanding of the molecular details of T cell exhaustion and the cytokine storm that are crucial for severe patients and the cause of death from COVID-19 [24, 25]. Extensions of the current model to include these details are certainly required, and challenging, for a better understanding of the disease progression, especially the prediction of clinical course and early warning of a COVID-19-induced cytokine storm. In addition, the proposed model framework can also be applied to study other coronaviruses as long as there is available data.

Methods

Collected data from the published literatures

Dataset 1: Clinical data on the incubation period of 69 COVID-19 patients from China. The data were collected from the literature [56, 57].

   Dataset 2: Clinical data of 41 COVID-19 patients from the Fifth Medical Center of PLA General Hospital in Beijing, China. The data were retrieved from the reference, which includes expression of exhaustion biomarkers, cytokines and T cell counts in 6 healthy donors, 29 mild and 12 severe patients [58].

   Dataset 3: Routine blood data from 107 severe patients including 58 survivors and 49 deaths after clinical treatment at the Renmin Hospital of Wuhan University, China. The data includes cytokines levels from 58 survivors and 49 deaths. All confirmed COVID-19 patients were severe before treatment [59].

   Dataset 4: Clinical data from 50 healthy donors and 157 COVID-19 patients including 117 moderate and 40 severe symptoms, were collected from Yale New Haven Hospital, United States. The data from 117 moderate cases and 40 severe cases includes cytokines, $CD4^+$ T cell and $CD8^+$ T cell count, and the percentage of naïve $CD4^+$ and $CD8^+$ T cells [60].

   Dataset 5: Single cell sequence data from 8 patients as moderate and 13 patients as critical from Charité-Universitätsmedizin Berlin and University Hospital Leipzig. Genomic data of immune cells or epithelial cells from 8 patients as moderate and 13 patients as critical are included in the dataset [61].

   Dataset 6: Proteomic data from 46 COVID-19 and 53 control individuals from Taizhou Hospital, China. Proteomic data of receptor proteins for SARS-CoV-2 are incorporated into the dataset [62]. We only found the data for neuropilin-1 (NRP1) that is one of the receptors for SARS-CoV-2 [63] so that receptor protein was approximately equivalent to NRP1.

   Dataset 7: Kinetic data of effector T cells from 707 COVID-19 patients from Tongji Hospital, Wuhan, China. This dataset involves T cells dynamics from patients with different symptom presentations such as moderate (410 cases), severe (206 cases) and critical (91 cases) in hospitalized patients [64].

   Dataset 1 was used to validate the definition of incubation period in our model. The model assumptions stemmed from data analysis to datasets 2, 3, 4 and 5. We estimated the distribution of receptor protein from dataset 6 and the part of the parameters in our model from dataset 7 (Details in S1 Text).

Mathematical formulation of the multi-scale model

The multi-scale model describes the evolution of viral dynamics and host immune response in respone to SARS-CoV-2 infection. The model was formulated using a set of differential equations for the intracellular virus RNA concentration X_{in}^i, interferons concentration $[IFNs]^i$, antiviral protein $[AVPs]^i (i = 1, 2, \cdots, N)$, extracellular virus RNA concentration X_{ex}, cell surface free receptor protein number $R^i (i = 1, 2, \cdots, N)$, cytokine concentration $[Cytokines]$, and the effector T cell density $[T_{effector}]$. The model equations are detailed below.

   Viral dynamics.   We assumed that each receptor protein on target cell surface can only bind to one spike protein of SARS-CoV-2, and the receptor protein is freed when SARS-CoV-2 releases its RNA into the host cell and the spike protein dissociates from the receptor protein. These processes give a flux v_1^i as

$$v_1^i = k_{on}(R_0^i - R^i)X_{ex} - k_{off}R^i \tag{1}$$

Here, k_{on} is the binding rate between SARS-CoV-2 and receptor, k_{off} is the dissociation rate

between SARS-CoV-2 and receptor, R_0^i represents the total number of receptor protein on the ith cell, and R^i represents the receptor proteins binding to SARS-CoV-2. We assumed that the total number of receptor proteins on each cell is a constant over time, however the number is variable for different cells, and obeys gamma distribution with parameters α_1 and α_2, i.e., $R_0^i \sim \Gamma(\alpha_1, \alpha_2)$ (details shown in Table A in S1 Text).

SARS-CoV-2 release its RNA to the host cell after the spike protein is bound to the receptor on the target cell. The influx (v_2^i) of RNA to the host cell is proportional to the bound receptor protein, and hence

$$v_2^i = k_{\text{in}} R^i \tag{2}$$

The receptor becomes free when the genomic RNA is released.

Inside infected cells, the RNA of SARS-CoV-2 directs RNA replication and viral assembly using organelles and synthases from the host cell. During the process of viral replication, interferon signaling pathway is activated to produce interferons (IFNs) and antiviral proteins (AVPs), resulting in limited viral replication. In our model, we assumed that there is a time delay in the processes of virus replication (τ_1) because the process includes multistep reactions, and the inhibition of viral replication is described by a Hill type function. Therefore, the influx of viral replication (v_3^i) is described as below:

$$v_3^i = \lambda_1 X_{\text{in}}^i(t - \tau_1) \frac{b_1 K_1^{m_1}}{K_1^{m_1} + ([\text{AVPs}]^i)^{m_1}} - \delta_1 X_{\text{in}}^i \tag{3}$$

Here $\lambda_1, \tau_1, b_1, m_1, \delta_1$ are constants (details shown in Table A in S1 Text).

With respect to interferons (IFNs), they are activated by viral RNA and exhibit positive autoregulation [29]. So, the influx of IFNs pure synthesis is

$$v_4^i = \lambda_2 X_{\text{in}}^i + b_2 \frac{([\text{IFNs}]^i)^{m_2}}{([\text{IFNs}]^i)^{m_2} + K_2^{m_2}} - \delta_2 [\text{IFNs}]^i \tag{4}$$

here m_2, K_2, δ_2 are constants (details shown in Table A in S1 Text).

Antiviral proteins (AVPs) are synthesized by stimulated IFN downstream signal pathways and are degraded naturally in the host cell. Hence, the influx of AVPs pure synthesis is

$$v_5^i = \lambda_3 [\text{IFNs}]^i - \delta_3 [\text{AVPs}]^i \tag{5}$$

here λ_3, δ_3 are constants (details in Table A in S1 Text).

Finally, progeny virus is assembled by organelles and synthases from the host cell after viral replication. Since this process involves multistep reactions, we assumed a lag time τ_2 for the process of viral budding, such that

$$v_6^i = q_0 X_{\text{in}}^i(t - \tau_2) \tag{6}$$

here q_0, τ_2 are constants (details shown in Table A in S1 Text).

Multi-cellular responses and cell infection. All SARS-CoV-2 particles released from host cells enter the extracellular environment. The extracellular virus can either bind to receptor proteins in target cells and infect the host cells, or are cleared from the body. There are many different types of cells in the tissue environment, and these cells may affect the identification and binding of SARS-CoV-2 to target cells that express the receptor. Biologically, it is not a trivial process to initiate an invading process of a cell by viruses. Cellular self-defense in target cells protects the cells against pathogens [65], and viruses in a nearby cell can induce signals to promote the binding between viral spike proteins and cell membrane proteins. Here, we

ignored the detail process and assumed a random process that extracellular viruses identify a target cell with a probability $\beta^i = \beta(X_{ex}, R_0^i, A)$ that depends on virus concentration outside the cell, cell membrane receptor protein number, and the binding affinity $A = k_{off}/k_{on}$. Hence, we write

$$\beta(X_{ex}, R_0^i, A) = \beta_0 \frac{(X_{ex}R_0^i)^{m_0}}{(K_0(A + X_{ex}))^{m_0} + (X_{ex}R_0^i)^{m_0}} \qquad (7)$$

here, K_0 is constant (details shown at Section 2.2 in S1 Text).

The binding affinity measures the equilibrium dissociation constant between the S protein on SARS-CoV-2 and the receptor protein on target cells. In our model, all cells are initially normal and uninfected, and once a cell is recognized by SARS-CoV-2 and the infection is initiated, the status of the cell becomes infected. Let $I(t) \subseteq \{1, 2, \cdots, N\}$ the index of infected cells at time t. Let v_{cell} denote the volume of a single cell, and V_{ex} denote the volume of extracellular environment, the above biological processes lead to the following differential equations.

$$\frac{dX_{ex}}{dt} = \frac{v_{cell}}{V_{ex}}\sum_{i \in I(t)} q_0 X_{in}^i(t - \tau_2) + \frac{1}{V_{ex}}\sum_{i \in I(t)}[k_{off}R^i - k_{on}(R_0^i - R^i)X_{ex}] - \delta_4 X_{ex} \qquad (8)$$

$$\frac{dR^i}{dt} = k_{on}(R_0^i - R^i)X_{ex} - k_{off}R^i - k_{in}R^i \qquad (9)$$

$$\frac{dX_{in}^i}{dt} = \frac{k_{in}R^i}{v_{cell}} + \lambda_1 X_{in}^i(t - \tau_1)\frac{b_1 K_1^{m_1}}{K_1^{m_1} + ([AVPs]^i)^{m_1}} - \delta_1 X_{in}^i - q_0 X_{in}^i(t - \tau_2) \qquad (10)$$

$$\frac{d[IFNs]^i}{dt} = \lambda_2 X_{in}^i + b_2 \frac{([IFNs]^i)^{m_2}}{([IFNs]^i)^{m_2} + K_2^{m_2}} - \delta_2[IFNs]^i \qquad (11)$$

$$\frac{d[AVPs]^i}{dt} = \lambda_3[IFNs]^i - \delta_3[AVPs]^i \qquad (12)$$

Here $v_{ex} = V_{ex}/N$ denotes the mean volume that a single cell occupies the extracellular environment. From the above equations, the viral dynamics and cellular responses are coupled using the indexes $I(t)$ of infected cells.

T cell response for clearing virus. Next, to model the T cell response to virus, we considered the cytokine concentration [Cytokines] and the effector cell number [$T_{effector}$], and assumed a constant naïve T number [T_0] over time. The infected cells secrete cytokines and activate the naïve T cells to produce effector T cells. The effector T cells continuously clear the infected cells and secrete cytokines, which may lead to chronic inflammation and further induce the exhaustion of effector cells. These processes are described by integrodifferential equations given below

$$\frac{d[T_{effector}]}{dt} = \mu_1[T_0]\frac{[Cytokines]^{m_3}}{[Cytokines]^{m_3} + K_3^{m_3}} - \delta_{effector}([Cytokines])[T_{effector}] \qquad (13)$$

$$\frac{d[Cytokines]}{dt} = \mu_2 R_{IC} + \mu_3[T_{effector}] - \delta_6[Cytokines] \qquad (14)$$

Here, R_{IC} denotes the ratio of infected cells to total cells.

The coefficient δ_{effector} ([Cytokines]) represents the rate of effector T cell exhaustion/cleaning, which is dependent on the chronic inflammatory environment due to the accumulation of cytokines. Hence, we assumed that δ_{effector} ([Cytokines]) depends on the accumulation of a Hill type function of [Cytokines] over a period of effective time [66], which is formulated as

$$\delta_{\text{effector}} \left([\text{Cytokines}] \right) = \delta_5 + \rho H(t - t_2) \int_{t-\tau_3}^{t} \frac{[\text{Cytokines}](s)^{m_4}}{[\text{Cytokines}](s)^{m_4} + K_4^{m_4}} \, ds \qquad (15)$$

here δ_5 is the basal cleaning rate, ρ is the maximum rate of T cell exhaustion, and τ_3 is the effective period of cytokines. The Heaviside function $H(t - t_2)$ is introduced to represent the starting of T cell exhaustion, where

$$H(t) = \begin{cases} 1 & t > 0 \\ 0 & t \leq 0 \end{cases} \qquad (16)$$

Here $t_2 = T_{\text{IP}}$ to indicates the starting time of T cell exhaustion from a symptomatic state. Clinically, T cell exhaustion is associated with the expression of specific immune-inhibitory factors including PD-1 and Tim-3 on the cell surface [20, 58], but the origin of T cell exhaustion remains unclear [23, 28]. Here, we simply introduced variables ρ and K_4 to model the effects of T cell exhaustion.

Finally, we assumed that infected cells are cleared by effector T cells and that the clearing rate is proportional to the effector T cell number, i.e., the clearing rate

$$\eta(t) = \eta_0 [T_{\text{effector}}] \qquad (17)$$

where η_0 is a constant rate. When an infected cell is cleared, a normal cell is generated to maintain the total cell number N.

Numerical scheme

The proposed multi-scale model was established using a combination of deterministic and random simulations. The schematic framework is summarized in (Fig 10).

The scheme starts with a tissue system of N normal cells and an initial extracellular SARS-CoV-2 concentration $X_{\text{ex}}(0) = X_{\text{ex},0}$. After viral infection, each cell undergoes state change from normal to infected, and is cleaned by effector T cells. When an infected cell is cleaned, a new normal cell is generated to replace the lost cell so that the total cell number N remains unchanged. All new normal cells exhibit heterogeneous cell surface receptor protein numbers that obey a gamma distribution $R_0^i \sim \Gamma(\alpha_1, \alpha_2)$.

In numerical simulations, we started from t = 0 and simulated the infection progression using a time step dt = 0.01h. At each time interval $[t, t + dt]$, the extracellular virus binds to the receptor proteins on target cells, releases the mRNA into the target cells, replicates the mRNAs and synthesizes new virus, and the intracellular viruses are released into the extracellular environment. Meanwhile, interferons (IFNs) and antiviral proteins (AVPs) are produced and inhibit viral replication in the host cell. These processes are simulated following Eqs (8)–(12). Each cell dynamically changes from normal to infected states following the infections process (Fig 10). At each time step, a normal cell has a probability $\beta(X_{\text{ex}}, R_0^i, A) \times dt$ of switching to an infected state and the index set $I(t)$ of infected cells changes over time. The T cell response is triggered by the infected cells (Fig 10). Infected cells secrete cytokines, such as IL-2, IL-6, TNF-α, etc., to induce the activation of naïve T cells. Effector T cells promote the cleaning of infected cells, and secrete cytokines, including IL-2, IL-6, TNF-α, etc. Eqs (13) and (14). The cytokines lead to the exhaustion of effector T cells following the exhaustion rate defined by
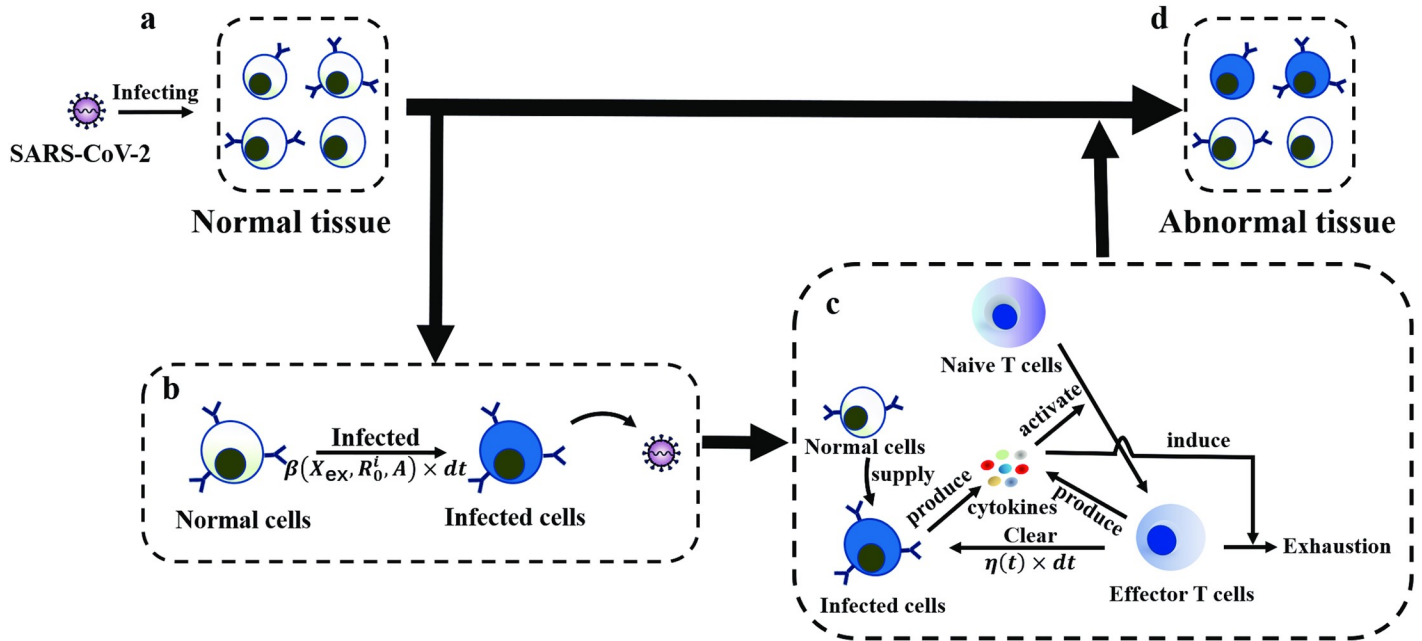
Fig 10. Schematic diagram for the multi-scale modeling of SARS-CoV-2 infection. a. Susceptible cells in normal tissue are infected by SARS-CoV-2. b. Cell states vary from normal to infected. Each normal cell becomes an infected cell with a probability of $\beta(X_{ex}, R_0^i, A) \times dt$, and the infected cell spreads virus to the microenvironment and further infect other susceptible cells. c. The T cell response is triggered by infected cells that secrete cytokines (such as ILs, TNFs, IFNs, etc.). Naïve T cells are activated by cytokines and produce effector T cells to clear infected cells. Meanwhile, the above Eqs (1)–(17) represent the multi-scale model in the current study. This model includes viral dynamics, IFN response, and T cell response after SARS-CoV-2 infection. The viral dynamics and IFN response are coupled through the indexes of infected cells, and the T cell response and cytokines are connected by the number of infected cells. Cytokines are produced by both infected cells and effector T cells, promoting T cell exhaustion. Infected cells are removed with a probability of $\eta(t) \times dt$. If an infected cell is cleared, a normal cell is generated to keep the total number of target cells unchanged. d. Normal tissue develops into abnormal tissue, and the severity is measured by the ratio of infected cells in the tissue.

https://doi.org/10.1371/journal.pcbi.1009587.g010

Eq (15). The infected cells are cleaned by effector T cells so that each infected cell is removed with a probability $\eta(t) \times dt$ during an interval $[t, t + dt]$. When an infected cell is cleaned, a new normal cell is generated to replace the lost cell.

The above processes suggest a numerical scheme shown below (Fig J in S1 Text):

1. **System initialization**: Set the time t = 0 and the step size (dt = 0.01h). Initialize the system states, including the total cell number ($N = 5000$), cell surface receptor protein numbers R_0^i (following the gamma distribution $\Gamma(\alpha_1, \alpha_2)$) in each cell, initial concentration of extracellular SARS-CoV-2 ($X_{ex,0}$), naïve T cell number ($[T_0]$), and the initial conditions $[X_{ex}](0) = X_{ex,0}, R^i(0) = 0, \ X_{in}^i(0) = 0, [IFNs]^i(0) = 0, [AVPs]^i(0) = 0, \ [Cytokines](0) = 0, \ [T_{effector}](0) = 0$. Set the states of all cells to be normal ($S_i = 0$), $N_{infected} = 0$ and the infected cells index I to be an empty set.

2. **Update cell states**: For i from 1 to N:

   a) If $S_i = 0$, changes the cell state to $S_i = 1$ with a probability $p_1 = \beta(X_{ex}, R_0^i, A) \times dt$. If the cell state is changed, the index i is added to the index set I.

   b) If $S_i = 1$, cleans the cell with a probability $p_2 = \eta(t) \times dt$. If the cell is cleaned, the cell state is reset with a newly generated receptor number $R_0^i \sim \Gamma(\alpha_1, \alpha_2)$ and the initial conditions $S_i = 0, R^i = 0, X_{in}^i = 0, [IFNs]^i = 0, [AVPs]^i = 0$.

   c) If $S_i = 1$ and is not cleaned, solve the differential equation for R^i, $[IFNs]^i$, $[AVPs]^i$ and X_{in}^i Eqs (9)–(12) for one step ($t \rightarrow t + dt$) using a difference method (e.g., DDE23 in

MATLAB), and update the intracellular SARS-CoV-2 concentration X_{in}^{i}, IFNs concentration $[\mathrm{IFNs}]^{i}$, and AVPs concentration $[\mathrm{AVPs}]^{i}$.

3. **Update extracellular environment and the host immune response**: Update the infected cells number N_{infected}, and solve the Eq (8) and Eqs (13)–(15) for one step ($t \to t + dt$) with updated index I and the number N_{infected}, and update the variables X_{ex},[Cytokines], $[T_{\mathrm{effector}}]$.

4. **Update the time**: Let t = t+dt, and either go to step 2 or terminate the simulation process.

Parameter estimations and sensitivity analysis

Some of the model parameters were obtained directly from published literature, i.e., the association (k_{on}) and dissociation (k_{off}) between S protein of SARS-CoV-2, receptor protein were taken as $k_{\mathrm{on}} = 0.6759 \mathrm{nM} \cdot \mathrm{h}^{-1}$ and $k_{\mathrm{off}} = 9.9365 \mathrm{h}^{-1}$ [67].

Other parameters were estimated by related studies. The mammalian cell volume (v_{cell}) is $100 \sim 10000 \mu\mathrm{m}^{3}$ [68] and the density of naïve T cell is approximately $4 \times 10^{-3} g/cm^{3}$ [69] so that the counts of naïve T cell ($[T_0]$) are about $0.4 \sim 4.0 \times 10^{5}$cells/ml. The half-life of IFNs, AVPs and SARS-CoV-2 were determined from published studies; the half-life of IFNs ranged from 1.3 to 4.7 hours [70], AVPs is 2~24 hours [29], and the half-life of SARS-CoV-2 is about 6.8 hours [71]. By the natural depletion rate $\delta = \ln 2/t_{1/2}$ ($t_{1/2}$ is the half-life), the degradation of IFNs, AVPs and SARS-CoV-2 were estimated as $\delta_1 = 0.1 \mathrm{h}^{-1}$, $\delta_2 = 0.4 \mathrm{h}^{-1}$, $\delta_3 = 0.12 \mathrm{h}^{-1}$, respectively. Extracellular viruses are easier to be clean by the humoral and cell-mediated immune response so that we set $\delta_4 = 2.5\delta_1 = 0.25 \mathrm{h}^{-1}$.

In Eq (7), parameters were set to $m_0 = 5$, $K_0 = 48 \times 10^{-11}$, $\beta_0 = 0.15$ to satisfy the effect of threshold between the virus and receptor protein (Fig Ka in S1 Text), R_0 in the Eq (1) was assumed to obey a gamma distribution $\Gamma(\alpha_1, \alpha_2)$ and the parameters of α_1, α_2 were estimated using the max likelihood estimation (MLE) ($\alpha_1 = 12.11$, $\alpha_2 = 9.50$) (Fig Kb in S1 Text).

We estimated other parameters by fitting simulation results with clinical data. We fitted clinical data of T cell dynamics from dataset 7 to estimate the remaining parameters and patients with different symptom presentation by varying the exhaustion rate (ρ) (Moderate: ρ = 0.0005; Severe: ρ = 0.0025; Critical: ρ = 0.005) (Fig L in S1 Text). Before fitting the data, we assumed that the initial time of patients in the hospital ($t = T_{\mathrm{IP}} + t_0$) and t_0 represents a time interval from showing symptom to being hospitalized. The parameter t_0 was taken as 1 day based on the information of dataset 7. The parameters were estimated within relevant biological ranges such that the number of effector T cells was well fitted to patients with different symptoms. A detailed description and default values of the model parameters are shown in Table A in S1 Text. In addition, we examined our model using two indexes: Q and L (the definitions of these indexes is in Section 3 in S1 Text). Details of model validation are provided in the Section 9 in S1 Text. The results displayed in Table C and Figs L and M in S1 Text suggest that the accumulation effect (15) is appropriate for true dynamics of effector T cells in COVID-19 patients.

We applied the method of partial rank correlation coefficient (PRCC) [72] to perform sensitivity analysis for estimated parameters related to viral dynamics. Sensitivity analysis was performed using 200 sample runs and a perturbation magnitude of 0.1. The sensitivities of input parameters to the ratio of infected cells (R_{IC}) on day 30 after infection were calculated (Fig D in S1 Text). The most sensitive parameters λ_1 and b_1 correspond to the rate of viral RNA replication and are attributed to the characteristics of the virus itself. The parameters λ_2 and K_1 are also significant, which correspond to IFN response and the coefficient of inhibiting viral

replication, respectively. We also note the two parameters v_{ex} and δ_4 that were associated with the process of susceptible cells infected by SARS-CoV-2.

Treatment model

The strategies of treatment for COVID-19 are primarily classified as antiviral treatment and immune modulation. Antiviral treatment methods include type I interferons and Arbidol [44], and immune modulations include immunoglobulins and hormone treatment [73]. Potential immune therapy, such as blocking the inhibitory immune checkpoint molecules, has been applied in severe cases [40]. To model the therapeutic effects, we considered four treatment strategies, including acceleration of IFN response, restriction of viral replication, promotion of extracellular virus clearance, and inhibition of T cell exhaustion. We introduced a quadruple $(\varepsilon_1, \varepsilon_2, \varepsilon_3, \varepsilon_4)$ to represent the effects of the above four strategies. Thus, the equations of the preceding model were modified as follows:

$$\frac{d[\text{IFNs}]^i}{dt} = (1 + \varepsilon_1)\lambda_2 X_{in}^i + b_2 \frac{([\text{IFNs}]^i)^{m_2}}{([\text{IFNs}]^i)^{m_2} + K_2^{m_2}} - \delta_2[\text{IFNs}]^i \tag{18}$$

$$\begin{aligned}
\frac{dX_{in}^i}{dt} &= \frac{k_{in}R^i}{v_{cell}} + \lambda_1 X_{in}^i(t - \tau_1) \frac{b_1((1 - \varepsilon_2)K_1)^{m_1}}{((1 - \varepsilon_2)K_1)^{m_1} + ([\text{AVPs}]^i)^{m_1}} \\
&\quad - \delta_1 X_{in}^i - q_0 X_{in}^i(t - \tau_2)
\end{aligned} \tag{19}$$

$$\begin{aligned}
\frac{dX_{ex}}{dt} &= \frac{v_{cell}}{V_{ex}} \sum_{i \in I(t)} q_0 X_{in}^i(t - \tau_2) + \frac{1}{V_{ex}} \sum_{i \in I(t)} [k_{off}R^i - k_{on}(R_0^i - R^i)X_{ex}] \\
&\quad - \delta_4(1 + \varepsilon_3)X_{ex}
\end{aligned} \tag{20}$$

$$\delta_{effector}([\text{Cytokines}]) = \delta_5 + \rho H(t - t_2) \int_{t-\tau_3}^{t} \frac{[\text{Cytokines}](s)^{m_4}}{[\text{Cytokines}](s)^{m_4} + ((1 + \varepsilon_4)K_4)^{m_4}} ds \tag{21}$$

Here, $\varepsilon_1(\varepsilon_1 > 0)$ represents acceleration of the IFN response, $\varepsilon_2(0 < \varepsilon_2 \leq 1)$ represents the restriction of viral replication, $\varepsilon_3 (\varepsilon_3 > 0)$ represents the promotion of extracellular virus clearance, and $\varepsilon_4 (\varepsilon_4 > 0)$ represents inhibition of T cell exhaustion. Moreover, we assumed that a patient starts the treatment on day $t_3 = 15$ after infection, so that the above equations were applied when $t \geq t_3$. The Eqs (18)–(21) were used to explore the treatment dynamics for COVID-19 patients.

Supporting information

S1 Text. Supplementary materials.
(PDF)

S2 Text. Source codes of the numerical scheme.
(PDF)

Acknowledgments

Author Contributions

Conceptualization: Zishu Pan, Jinzhi Lei, Xiufen Zou.

Data curation: Mengqian Hao.

Formal analysis: Shun Wang, Mengqian Hao.

Funding acquisition: Xiufen Zou.

Investigation: Shun Wang, Mengqian Hao.

Methodology: Shun Wang, Jinzhi Lei, Xiufen Zou.

Project administration: Zishu Pan, Xiufen Zou.

Resources: Xiufen Zou.

Software: Shun Wang.

Supervision: Xiufen Zou.

Validation: Shun Wang.

Visualization: Shun Wang, Mengqian Hao.

Writing – original draft: Shun Wang, Zishu Pan, Jinzhi Lei, Xiufen Zou.

Writing – review & editing: Zishu Pan, Jinzhi Lei, Xiufen Zou.

References

1. Huang C, Wang Y, Li X, Ren L, Zhao J, Hu Y, et al. Clinical features of patients infected with 2019 novel coronavirus in Wuhan, China. The Lancet. 2020; 395(10223):497–506. https://doi.org/10.1016/S0140-6736(20)30183-5

2. Xu Z, Shi L, Wang Y, Zhang J, Huang L, Zhang C, et al. Pathological findings of COVID-19 associated with acute respiratory distress syndrome. The Lancet Respiratory Medicine. 2020; 8(4):420–422. https://doi.org/10.1016/S2213-2600(20)30076-X PMID: 32085846

3. Wang X, Gui J. Cell-mediated immunity to SARS-CoV-2. Pediatric Investigation. 2020; 4(4):281–291. https://doi.org/10.1002/ped4.12228 PMID: 33376956

4. Qin C, Zhou L, Hu Z, Zhang S, Yang S, Tao Y, et al. Dysregulation of Immune Response in Patients With Coronavirus 2019 (COVID-19) in Wuhan, China. Clinical Infectious Diseases. 2020; 71(15):762–768. https://doi.org/10.1093/cid/ciaa248 PMID: 32161940

5. Tan M, Liu Y, Zhou R, Deng X, Li F, Liang K, et al. Immunopathological characteristics of coronavirus disease 2019 cases in Guangzhou, China. Immunology. 2020; 160(3):261–268. https://doi.org/10.1111/imm.13223 PMID: 32460357

6. Cao Q, Chen YC, Chen CL, Chiu CH. SARS-CoV-2 infection in children: Transmission dynamics and clinical characteristics. Journal of the Formosan Medical Association. 2020; 119(3):670–673. https://doi.org/10.1016/j.jfma.2020.02.009 PMID: 32139299

7. Lee PI, Hu YL, Chen PY, Huang YC, Hsueh PR. Are children less susceptible to COVID-19? Journal of Microbiology, Immunology and Infection. 2020; 53(3):371–372. https://doi.org/10.1016/j.jmii.2020.02.011 PMID: 32147409

8. Hu Z, Song C, Xu C, Jin G, Chen Y, Xu X, et al. Clinical characteristics of 24 asymptomatic infections with COVID-19 screened among close contacts in Nanjing, China. medRxiv. 2020; 63(5):706–711. https://doi.org/10.1007/s11427-020-1661-4 PMID: 32146694

9. Wang Z, Pan H, Jiang B. Type I IFN deficiency: an immunological characteristic of severe COVID-19 patients. Signal Transduction and Targeted Therapy. 2020; 5(1):1–2. https://doi.org/10.1038/s41392-020-00306-4 PMID: 32929061

10. Rothe C, Schunk M, Sothmann P, Bretzel G, Froeschl G, Wallrauch C, et al. Transmission of 2019-nCoV Infection from an Asymptomatic Contact in Germany. New England Journal of Medicine. 2020; 382(10):970–971. https://doi.org/10.1056/NEJMc2001468 PMID: 32003551

11. Hamming I, Timens W, Bulthuis M, Lely A, Navis G, van Goor H. Tissue distribution of ACE2 protein, the functional receptor for SARS coronavirus. A first step in understanding SARS

pathogenesis. The Journal of Pathology. 2004; 203(2):631–637. https://doi.org/10.1002/path.1570 PMID: 15141377

12. Lamers MM, Beumer J, van der Vaart J, Knoops K, Puschhof J, Breugem TI, et al. SARS-CoV-2 productively infects human gut enterocytes. Science. 2020; 369(6499):50–54. https://doi.org/10.1126/science.abc1669 PMID: 32358202

13. Lukassen S, Chua RL, Trefzer T, Kahn NC, Schneider MA, Muley T, et al. SARS-CoV-2 receptor ACE2 and TMPRSS2 are primarily expressed in bronchial transient secretory cells. The EMBO Journal. 2020; 39(10). https://doi.org/10.15252/embj.20105114 PMID: 32246845

14. Harrison AG, Lin T, Wang P. Mechanisms of SARS-CoV-2 Transmission and Pathogenesis. Trends in Immunology. 2020; 41(12):1100–1115. https://doi.org/10.1016/j.it.2020.10.004 PMID: 33132005

15. Janeway CA, Medzhitov R. Innate Immune Recognition. Annual Review of Immunology. 2002; 20 (1):197–216. https://doi.org/10.1146/annurev.immunol.20.083001.084359 PMID: 11861602

16. Lazear HM, Schoggins JW, Diamond MS. Shared and Distinct Functions of Type I and Type III Interferons. Immunity. 2019; 50(4):907–923. https://doi.org/10.1016/j.immuni.2019.03.025 PMID: 30995506

17. Wu C, Chen X, Cai Y, Xia J, Zhou X, Xu S, et al. Risk Factors Associated With Acute Respiratory Distress Syndrome and Death in Patients With Coronavirus Disease 2019 Pneumonia in Wuhan, China. JAMA Internal Medicine. 2020; 180(7):934. https://doi.org/10.1001/jamainternmed.2020.0994 PMID: 32167524

18. Zhou F, Yu T, Du R, Fan G, Liu Y, Liu Z, et al. Clinical course and risk factors for mortality of adult inpatients with COVID-19 in Wuhan, China: a retrospective cohort study. The Lancet. 2020; 395 (10229):1054–1062. https://doi.org/10.1016/S0140-6736(20)30566-3 PMID: 32171076

19. Chen Z, John Wherry E. T cell responses in patients with COVID-19. Nature Reviews Immunology. 2020; 20(9):529–536. https://doi.org/10.1038/s41577-020-0402-6 PMID: 32728222

20. Diao B, Wang C, Tan Y, Chen X, Liu Y, Ning L, et al. Reduction and Functional Exhaustion of T Cells in Patients With Coronavirus Disease 2019 (COVID-19). Frontiers in Immunology. 2020; 11(May):1–7.

21. Liu Y, Yang Y, Zhang C, Huang F, Wang F, Yuan J, et al. Clinical and biochemical indexes from 2019-nCoV infected patients linked to viral loads and lung injury. Science China Life Sciences. 2020; 63 (3):364–374. https://doi.org/10.1007/s11427-020-1643-8 PMID: 32048163

22. Sominsky L, Walker DW, Spencer SJ. One size does not fit all–Patterns of vulnerability and resilience in the COVID-19 pandemic and why heterogeneity of disease matters. Brain, behavior, and immunity. 2020; 87:1. https://doi.org/10.1016/j.bbi.2020.03.016 PMID: 32205119

23. Wherry EJ. T cell exhaustion. Nature Immunology. 2011; 12(6):492–499. https://doi.org/10.1038/ni.2035 PMID: 21739672

24. Hu B, Huang S, Yin L. The cytokine storm and COVID-19. Journal of Medical Virology. 2021; 93 (1):250–256. https://doi.org/10.1002/jmv.26232 PMID: 32592501

25. Mahmudpour M, Roozbeh J, Keshavarz M, Farrokhi S, Nabipour I. COVID-19 cytokine storm: The anger of inflammation. Cytokine. 2020; 133:155151. https://doi.org/10.1016/j.cyto.2020.155151 PMID: 32544563

26. Noroozi R, Branicki W, Pyrc K, Labaj PP, Pospiech E, Taheri M, et al. Altered cytokine levels and immune responses in patients with SARS-CoV-2 infection and related conditions. Cytokine. 2020; 133:155143. https://doi.org/10.1016/j.cyto.2020.155143 PMID: 32460144

27. Fajgenbaum DC, June CH. Cytokine Storm. New England Journal of Medicine. 2020; 383(23):2255–2273. https://doi.org/10.1056/NEJMra2026131 PMID: 33264547

28. Pauken KE, Wherry EJ. SnapShot: T Cell Exhaustion. Cell. 2015; 163(4):1038–1038.e1. https://doi.org/10.1016/j.cell.2015.10.054 PMID: 26544946

29. Tan J, Pan R, Qiao L, Zou X, Pan Z. Modeling and Dynamical Analysis of Virus-Triggered Innate Immune Signaling Pathways. PLoS ONE. 2012; 7(10). https://doi.org/10.1371/journal.pone.0048114 PMID: 23118935

30. Oberfeld B, Achanta A, Carpenter K, Chen P, Gilette NM, Langat P, et al. SnapShot: COVID-19. Cell. 2020; 181(4):954–954.e1. https://doi.org/10.1016/j.cell.2020.04.013 PMID: 32413300

31. Wiersinga WJ, Rhodes A, Cheng AC, Peacock SJ, Prescott HC. Pathophysiology, Transmission, Diagnosis, and Treatment of Coronavirus Disease 2019 (COVID-19): A Review. JAMA—Journal of the American Medical Association. 2020; 324(8):782–793. https://doi.org/10.1001/jama.2020.12839 PMID: 32648899

32. WHO. WHO siterep 73. World Health Organization. 2020; 2019(March):2633.

33. Hadjadj J, Yatim N, Barnabei L, Corneau A, Boussier J, Smith N, et al. Impaired type I interferon activity and inflammatory responses in severe COVID-19 patients. Science. 2020; 369(6504):718–724. https://doi.org/10.1126/science.abc6027 PMID: 32661059

34. Zhang Q, Liu Z, Moncada-Velez M, Chen J, Ogishi M, Bigio B, et al. Inborn errors of type I IFN immunity in patients with life-threatening COVID-19. Science. 2020; 370 (6515). https://doi.org/10.1126/science.abd4570

35. Sanders JM, Monogue ML, Jodlowski TZ, Cutrell JB. Pharmacologic Treatments for Coronavirus Disease 2019 (COVID-19): A Review. JAMA—Journal of the American Medical Association. 2020; 323 (18):1824–1836. PMID: 32282022

36. Kusnadi A, Ramírez-Suástegui C, Fajardo V, Chee SJ, Meckiff BJ, Simon H, et al. Severely ill COVID-19 patients display impaired exhaustion features in SARS-CoV-2-reactive CD8+ T cells. Science immunology. 2021; 6(55):1–19. https://doi.org/10.1126/sciimmunol.abe4782 PMID: 33478949

37. Acharya D, Liu GQ, Gack MU. Dysregulation of type I interferon responses in COVID-19. Nature Reviews Immunology. 2020; 20(7):397–398. https://doi.org/10.1038/s41577-020-0346-x PMID: 32457522

38. Rydyznski Moderbacher C, Ramirez SI, Dan JM, Grifoni A, Hastie KM, Weiskopf D, et al. Antigen-Specific Adaptive Immunity to SARS-CoV-2 in Acute COVID-19 and Associations with Age and Disease Severity. Cell. 2020; 183(4):996–1012.e19. https://doi.org/10.1016/j.cell.2020.09.038 PMID: 33010815

39. Schwartz MD, Emerson SG, Punt J, Goff WD. Decreased naïve T-cell production leading to cytokine storm as cause of increased COVID-19 severity with comorbidities. Aging and Disease. 2020; 11 (4):742–745. https://doi.org/10.14336/AD.2020.0619 PMID: 32765940

40. Riva G, Nasillo V, Tagliafico E, Trenti T, Luppi M. COVID-19: room for treating T cell exhaustion? Critical Care. 2020; 24(1):229. https://doi.org/10.1186/s13054-020-02960-0 PMID: 32414395

41. Vivarelli S, Falzone L, Torino F, Scandurra G, Russo G, Bordonaro R, et al. Immune-checkpoint inhibitors from cancer to COVID-19: A promising avenue for the treatment of patients with COVID-19 (Review). International Journal of Oncology. 2021; 58(2):145–157. https://doi.org/10.3892/ijo.2020.5159 PMID: 33491759

42. Channappanavar R, Perlman S. Pathogenic human coronavirus infections: causes and consequences of cytokine storm and immunopathology. Seminars in Immunopathology. 2017; 39(5):529–539. https://doi.org/10.1007/s00281-017-0629-x PMID: 28466096

43. Glushkov RG, Gus' kova TA, LIu K, Nikolaeva IS. Mechanisms of arbidole's immunomodulating action. Vestnik Rossiiskoi akademii meditsinskikh nauk. 1999;(3):36–40. PMID: 10222830

44. Runan WEI, ZHENG N, JIANG X, Chunlian MA, Xiaowei XU, Shourong LIU, et al. Early antiviral therapy of abidor combined with lopinavir/ritonavir and re-combinant interferonα-2b in patients with novel coronavirus pneumonia in Zhejiang: A multicenter and prospective study. Chinese Journal of Clinical Infectious Diseases. 2020; p. E010–E010.

45. Wang R, Chen J, Hozumi Y, Yin C, Wei GW. Decoding Asymptomatic COVID-19 Infection and Transmission. The Journal of Physical Chemistry Letters. 2020; 11(23):10007–10015. https://doi.org/10.1021/acs.jpclett.0c02765 PMID: 33179934

46. Severa M, Diotti RA, Etna MP, Rizzo F, Fiore S, Ricci D, et al. Differential plasmacytoid dendritic cell phenotype and type I Interferon response in asymptomatic and severe COVID-19 infection. PLOS Pathogens. 2021; 17(9):e1009878. https://doi.org/10.1371/journal.ppat.1009878 PMID: 34473805

47. Zheng HY, Zhang M, Yang CX, Zhang N, Wang XC, Yang XP, et al. Elevated exhaustion levels and reduced functional diversity of T cells in peripheral blood may predict severe progression in COVID-19 patients. Cellular and Molecular Immunology. 2020; 17(5):541–543. https://doi.org/10.1038/s41423-020-0401-3 PMID: 32203186

48. Wherry EJ, Kurachi M. Molecular and cellular insights into T cell exhaustion. Nature Reviews Immunology. 2015; 15(8):486–499. https://doi.org/10.1038/nri3862 PMID: 26205583

49. Gandhi RT, Lynch JB, del Rio C. Mild or Moderate Covid-19. New England Journal of Medicine. 2020; 383(18):1757–1766. https://doi.org/10.1056/NEJMcp2009249

50. Wan S, Xiang Y, Fang W, Zheng Y, Li B, Hu Y, et al. Clinical features and treatment of COVID-19 patients in northeast Chongqing. Journal of Medical Virology. 2020; 92(7):797–806. https://doi.org/10.1002/jmv.25783 PMID: 32198776

51. Chen J, Vitetta L. Increased PD-L1 Expression May Be Associated With the Cytokine Storm and CD8+ T-Cell Exhaustion in Severe COVID-19. The Journal of Infectious Diseases. 2021; 223(9):1659–1660. https://doi.org/10.1093/infdis/jiab061 PMID: 33524110

52. Bertozzi AL, Franco E, Mohler G, Short MB, Sledge D. The challenges of modeling and forecasting the spread of COVID-19. Proceedings of the National Academy of Sciences of the United States of America. 2020; 117(29):16732–16738. https://doi.org/10.1073/pnas.2006520117 PMID: 32616574

53. Jewell NP, Lewnard JA, Jewell BL. Predictive Mathematical Models of the COVID-19 Pandemic. JAMA. 2020; 323(19):1893. https://doi.org/10.1001/jama.2020.6585 PMID: 32297897

54. Goyal A, Cardozo-Ojeda EF, Schiffer JT. Potency and timing of antiviral therapy as determinants of duration of SARS-CoV-2 shedding and intensity of inflammatory response. Science Advances. 2020; 6 (47):eabc7112. https://doi.org/10.1126/sciadv.abc7112 PMID: 33097472

55. Jenner AL, Aogo RA, Alfonso S, Crowe V, Deng X, Smith AP, et al. COVID-19 virtual patient cohort suggests immune mechanisms driving disease outcomes. PLOS Pathogens. 2021; 17(7):e1009753. https://doi.org/10.1371/journal.ppat.1009753 PMID: 34260666

56. Backer JA, Klinkenberg D, Wallinga J. Incubation period of 2019 novel coronavirus (2019-nCoV) infections among travellers from Wuhan, China, 20–28 January 2020. Eurosurveillance. 2020; 25(5):1–6. https://doi.org/10.2807/1560-7917.ES.2020.25.5.2000062 PMID: 32046819

57. Linton N, Kobayashi T, Yang Y, Hayashi K, Akhmetzhanov A, Jung Sm, et al. Incubation Period and Other Epidemiological Characteristics of 2019 Novel Coronavirus Infections with Right Truncation: A Statistical Analysis of Publicly Available Case Data. Journal of Clinical Medicine. 2020; 9(2):538. https://doi.org/10.3390/jcm9020538

58. Song JW, Zhang C, Fan X, Meng FP, Xu Z, Xia P, et al. Immunological and inflammatory profiles in mild and severe cases of COVID-19. Nature Communications. 2020; 11(1). https://doi.org/10.1038/s41467-020-17240-2 PMID: 32641700

59. Dai Kai, Bao Anyu, Ye Peng, Xu Ming, Zhang Qinran, Zhou Yu, Jiang Wanli, Jiang Wubian, Wang Huimin, Zhu Mengfei, Tang Lingling, Zhu Chengliang, Xia Yuchen, Jiang Ying'an, Zou Xiufen LL. Risk factors for fatal outcome in patients with severe COVID-19: an analysis of 107 cases in Wuhan. Chin J Clin Infect Dis. 2020; 13(04):257–263.

60. Lucas C, Wong P, Klein J, Castro TBR, Silva J, Sundaram M, et al. Longitudinal analyses reveal immunological misfiring in severe COVID-19. Nature. 2020; 584(7821):463–469. https://doi.org/10.1038/s41586-020-2588-y PMID: 32717743

61. Chua RL, Lukassen S, Trump S, Hennig BP, Wendisch D, Pott F, et al. COVID-19 severity correlates with airway epithelium–immune cell interactions identified by single-cell analysis. Nature Biotechnology. 2020; 38(8):970–979. https://doi.org/10.1038/s41587-020-0602-4 PMID: 32591762

62. Shen B, Yi X, Sun Y, Bi X, Du J, Zhang C, et al. Proteomic and Metabolomic Characterization of COVID-19 Patient Sera. Cell. 2020; 182(1):59–72.e15. https://doi.org/10.1016/j.cell.2020.05.032 PMID: 32492406

63. Daly JL, Simonetti B, Klein K, Chen KE, Williamson MK, Antón-Plágaro C, et al. Neuropilin-1 is a host factor for SARS-CoV-2 infection. Science. 2020; 370(6518):861–865. https://doi.org/10.1126/science.abd3072 PMID: 33082294

64. Zhang B, Yue D, Wang Y, Wang F, Wu S, Hou H. The dynamics of immune response in COVID-19 patients with different illness severity. Journal of Medical Virology. 2021; 93(2):1070–1077. https://doi.org/10.1002/jmv.26504 PMID: 32910461

65. Randow F, MacMicking JD, James LC. Cellular self-defense: How cell-autonomous immunity protects against pathogens. Science. 2013; 340(6133):701–706. https://doi.org/10.1126/science.1233028 PMID: 23661752

66. Gu C, Zhang J, Chen Y, Lei J. A trigger model of apoptosis induced by tumor necrosis factor signaling. BMC Systems Biology. 2011; 5(SUPPL. 1):1–10. https://doi.org/10.1186/1752-0509-5-S1-S13 PMID: 21689472

67. Wrapp D, Wang N, Corbett KS, Goldsmith JA, Hsieh CL, Abiona O, et al. Cryo-EM structure of the 2019-nCoV spike in the prefusion conformation. Science. 2020; 367(6483):1260–1263. https://doi.org/10.1126/science.abb2507 PMID: 32075877

68. Moran U, Phillips R, Milo R. SnapShot: Key numbers in biology. Cell. 2010; 141(7):1–2. https://doi.org/10.1016/j.cell.2010.06.019 PMID: 20603006

69. Lai X, Stiff A, Duggan M, Wesolowski R, Carson WE, Friedman A. Modeling combination therapy for breast cancer with BET and immune checkpoint inhibitors. Proceedings of the National Academy of Sciences of the United States of America. 2018; 115(21):5534–5539. https://doi.org/10.1073/pnas.1721559115 PMID: 29735668

70. Vitale G, van Koetsveld PM, de Herder WW, van der Wansem K, Janssen JAMJL, Colao A, et al. Effects of type I interferons on IGF-mediated autocrine/paracrine growth of human neuroendocrine tumor cells. American Journal of Physiology-Endocrinology and Metabolism. 2009; 296(3):E559–E566. https://doi.org/10.1152/ajpendo.90770.2008 PMID: 19141687

71. Matson MJ, Yinda CK, Seifert SN, Bushmaker T, Fischer RJ, van Doremalen N, et al. Effect of Environmental Conditions on SARS-CoV-2 Stability in Human Nasal Mucus and Sputum. Emerging Infectious Diseases. 2020; 26(9):2276–2278. https://doi.org/10.3201/eid2609.202267 PMID: 32511089

72. Marino S, Hogue IB, Ray CJ, Kirschner DE. A methodology for performing global uncertainty and sensitivity analysis in systems biology. Journal of Theoretical Biology. 2008; 254(1):178–196. https://doi.org/10.1016/j.jtbi.2008.04.011 PMID: 18572196

73. Felsenstein S, Herbert JA, McNamara PS, Hedrich CM. COVID-19: Immunology and treatment options. Clinical Immunology. 2020; 215(April):108448. https://doi.org/10.1016/j.clim.2020.108448 PMID: 32353634